AD-A064 217 ARMY MISSILE RESEARCH AND DEVELOPMENT COMMAND REDSTO--ETC F/G 14/2
A COMPUTERIZED ACOUSTICAL ARRAY SYSTEM TO TEST BONDED RADOME JO--ETC(U)
OCT 78 J A SCHAEFFEL, V G IRELAN

UNCLASSIFIED DRDMI-T-78-96 NL

| OF |
AD
A064217

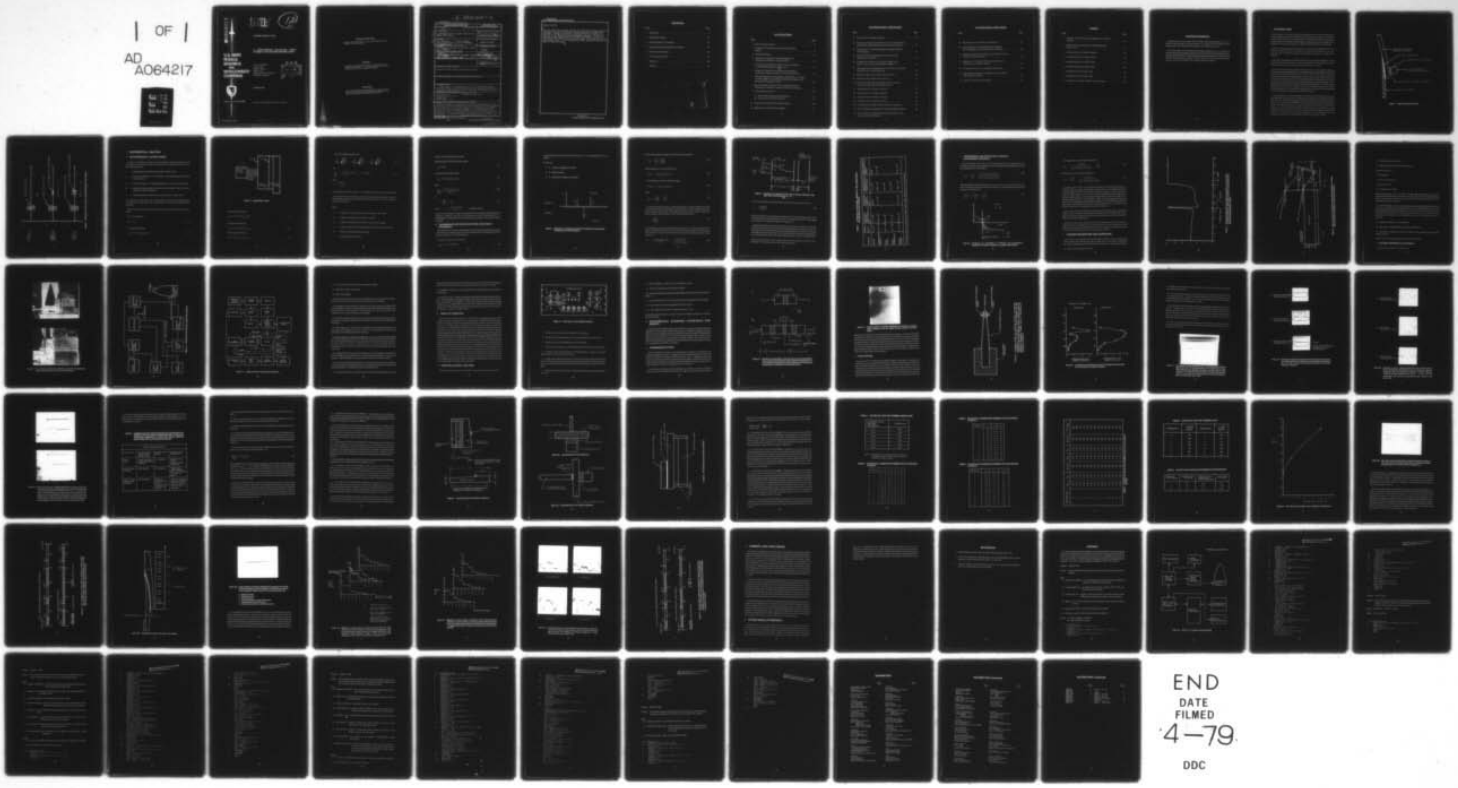

END
DATE
FILMED
4-79
DDC

LEVEL II

12
NW

TECHNICAL REPORT T-78-96

A COMPUTERIZED ACOUSTICAL ARRAY SYSTEM TO TEST BONDED RADOME JOINTS

John A. Schaeffel, Jr.
Virgil G. Irelan
Bobby R. Mullinix
Martin D. Fox
Missile Structures Directorate
Technology Laboratory

U.S. ARMY MISSILE RESEARCH AND DEVELOPMENT COMMAND

Redstone Arsenal, Alabama 35809

5 October 1978

Approved for Public Release; Distribution Unlimited.

DISPOSITION INSTRUCTIONS

DESTROY THIS REPORT WHEN IT IS NO LONGER NEEDED. DO NOT RETURN IT TO THE ORIGINATOR.

DISCLAIMER

THE FINDINGS IN THIS REPORT ARE NOT TO BE CONSTRUED AS AN OFFICIAL DEPARTMENT OF THE ARMY POSITION UNLESS SO DESIGNATED BY OTHER AUTHORIZED DOCUMENTS.

TRADE NAMES

USE OF TRADE NAMES OR MANUFACTURERS IN THIS REPORT DOES NOT CONSTITUTE AN OFFICIAL INDORSEMENT OR APPROVAL OF THE USE OF SUCH COMMERCIAL HARDWARE OR SOFTWARE.

(14) DRDMI-T-78-96

UNCLASSIFIED
SECURITY CLASSIFICATION OF THIS PAGE *(When Data Entered)*

REPORT DOCUMENTATION PAGE	READ INSTRUCTIONS BEFORE COMPLETING FORM
1. REPORT NUMBER: T-78-96 / 2. GOVT ACCESSION NO.	3. RECIPIENT'S CATALOG NUMBER
4. TITLE *(and Subtitle)*: (6) A COMPUTERIZED ACOUSTICAL ARRAY SYSTEM TO TEST BONDED RADOME JOINTS.	5. TYPE OF REPORT & PERIOD COVERED: (7) Final Technical Report,
	6. PERFORMING ORG. REPORT NUMBER
7. AUTHOR(s): (10) John A. Schaeffel, Jr., Virgil G. Irelan, Bobby R. Mullinix, Martin D. Fox, ~~University~~ of Connecticut	8. CONTRACT OR GRANT NUMBER(s): ~~DAAK40-77-C-0028~~
9. PERFORMING ORGANIZATION NAME AND ADDRESS: Commander, US Army Missile Research and Development Command, Attn: DRDMI-TLA, Redstone Arsenal, Alabama 35809	10. PROGRAM ELEMENT, PROJECT, TASK AREA & WORK UNIT NUMBERS: ~~3773138~~
11. CONTROLLING OFFICE NAME AND ADDRESS: Commander, US Army Missile Research and Development Command, Attn: DRDMI-TI, Redstone Arsenal, Alabama 35809	12. REPORT DATE: (11) 5 October ~~1978~~
	13. NUMBER OF PAGES: ~~77~~ (12) 79 p.
14. MONITORING AGENCY NAME & ADDRESS *(if different from Controlling Office)*	15. SECURITY CLASS. *(of this report)*: Unclassified
	15a. DECLASSIFICATION/DOWNGRADING SCHEDULE

16. DISTRIBUTION STATEMENT *(of this Report)*

Approved for Public Release; Distribution Unlimited.

17. DISTRIBUTION STATEMENT *(of the abstract entered in Block 20, if different from Report)*

18. SUPPLEMENTARY NOTES

"This project was accomplished as part of the US Army manufacturing technology program. The primary objective of this program is to develop, on a timely basis, manufactruing processes, techniques, and equipment for use in production of Army Materiel."

19. KEY WORDS *(Continue on reverse side if necessary and identify by block number)*

Acoustical Array
Nondestructive Test System
Computerized
Missile Radome Joints
Bondline Flaw Detection

20. ABSTRACT *(Continue on reverse side if necessary and identify by block number)*

Ceramic randomes are tested using an ultrasonic transducer array in the vicinity of the randome attachment ring bond line where the structural problems are particularly great. The array consists of 14 one-fourth inch transducers in line, with water couplant and operating in a 2.25 MWZ pulse/echo mode. Mechanical rotation of the radome generates the scan axis along the radome circumference. Flaws are determined by the character of the ultrasonic echo from the bond line. The resolution limit is one-fourth inch with one-fourth inch transducers.

(Continued on next page)

DD FORM 1 JAN 73 1473 EDITION OF 1 NOV 65 IS OBSOLETE

UNCALSSIFIED
SECURITY CLASSIFICATION OF THIS PAGE *(When Data Entered)*

393427

Abstract (cont'd)

If better resolution is desired one eight inch steps can be taken in both the horizontal and vertical directions to obtain approximately one eighth inch resolution. Displays are presented on storage monitors and computer plots. Each scan of the radome joint takes approximately one minute. Studies are presented of flaw characteristics and transducer phenomena. The results of these studies show clearly that the array is capable of differentiating three major types of flaws: silica inclusions and cracks, adhesive silica flaws, and adhesive fiberglass flaws.

CONTENTS

Section		Page
1.	Introduction	7
2.	Mathematical Analysis	10
3.	System Description and Operation	19
4.	Experimental Scanning Techniques and Results	29
5.	Summary and Conclusions	58
6.	Future Areas of Research	58
	References	60
	Appendix	61

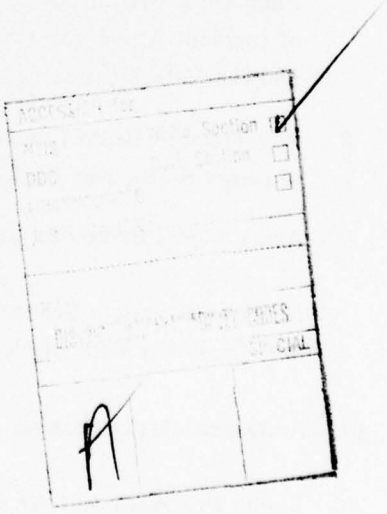

ILLUSTRATIONS

Figure — Page

1. Basic Transducer Geometry 8
2. Comparison of Echo Returns Characterizing Glue Bond Integrity 9
3. Insonification Model 11
4. Geometry for Calculation of Pressure Reflection and Transmission Coefficients at Normal Incidence 14
5. Geometry for Calculation of the Ratio of the Glue Reflection to the Water-Silica Reflection P_{glue}/V_1+P_1+ 16
   P_{refl}
6. Geometry for Calculation of Reflection and Transmission Coefficients at Oblique Incidence to a Liquid-Solid Interface 18
7. Theoretical Magnitude of the Reflection Coefficient $|V|$ as a Function of Incident Angle, for a Silica-Water Interface Using Equation (20) and the Values Contained in Table 1 20
8. Ray Trace of Beam Envelope From Transmitting Transducer, Through Silica, and Back to Transducer. Worse Case Conditions 21
9. Array Signal Processor Unit 23
   A. Entire System Scanning Pershing II Radome 23
   B. Close-Up View of Control Electronics 23
10. Acoustical Array Scanner System Block Diagram 24
11. Signal Processor and Array Block Diagram 25

ILLUSTRATIONS (CONTINUED)

Figure Page

12. Front Panel of Array Signal Processor 28

13. Geometry for Calculation of the Ratio (V_2/V_1) of the Transmission with a Radome Inserted Between Two Ultrasound Transducers 30

14. Typical Section of Neutron Radiograph of Pershing II Radome Under Inspection 31

15. Transducer Holder for Obtaining Ultrasonic Transmission Measurements on Radomes 32

16. Transmission Coefficients as a Function of Height on the Bond Line for Two Locations on Radome Number 1 33

17. Photograph of Flaws Manufactured in a Test Slab Using a *Dremel* Mono-Tool with 1/4 Inch Boring Tool 34

18. Detection of Silica Flaw Using the Ultrasonic Array 35

19. Detection of Silica-Adhesive Bond Line Flaw 36

20. Echo From (a) Over Fiberglass-Adhesive Flaw and (b) From the Adjacent Point With a Good Adhesive Joint 37

21. Acoustical Scan Test Number 1 Geometry 41

22. Acoustical Scan Test Number 2 Geometry 42

23. Acoustical Scan Test Number 3 Geometry 42

24. Acoustical Scan Test Number 4 Geometry 43

25. S/N Ratio Versus Number of Scan Averages of Transducer 0 49

26. *360° Glue Bond Line Inspection of Fractured Pershing II Radome* 50

27. 360° Comparison of Bond Faults In Pershing II Radome Using Acoustic and Manual Inspection 51

ILLUSTRATIONS (CONCLUDED)

Figure | Page

28. Orientation of Array at the Base of the Radome 52

29. Typical Sequence of Echoes Obtained with Transducer 0111 at 2.00 Inches on the Glue Bond Line of Radome I 53

30. Mapping of Front Surface to Bond Line Echo Ratios for Three Positions on Radome Number 1 54

31. Mapping of Front Surface to Bond Line Echo Ratios for Three Positions on Radome Number 2 55

32. *Acoustical Echo Level from* Fiberglass-Glue Bond Line 56

33. Flawed Regions Detected by Transducer 0 Located .725 Inch from the Base of the Silica 57

34. System for Computer Data Processing 62

TABLES

Table — Page

1. Acoustical Velocities, Densities and Impedances for Materials of Interest 17

2. Summary of Echo Characteristics to Differentiate Major Types of Flaws 38

3. Acoustical Scan Test Number 2 Resolution 45

4. Acoustical Scanner Test Number 4 Data 45

5. Acoustical Scanner Test Number 4 Data 46

6. Acoustical Scanner Test Number 4 Data 46

7. Acoustical Scan Test Number 5 Data 47

8. Acoustical Scan Test Number 5 Data 48

9. S/N Ratio as a Function of Number of Scan Averages 48

ACKNOWLEDGMENTS

The authors hereby express their sincere gratitude and deep appreciation to Mr. P. A. Ormsby for his assistance with the specimen, Dr. J. G. Castle for his consultation on this project and Ms. D. K. Russell for her assistance with the laboratory work.

The contract support of the in-house effort from Sperry Support Services on the electronic and mechanical hardware design and fabrication was timely and of excellent quality. Credit is especially due Mr. Michael E. Casciola who served as project engineer, Mr. David Himes for electronics and documentation support, Mr. Phil Catlett, J. B. Cecil and J. Chance for design support, and Mr. Howard Shahan for mechanical fabrication support.

1. INTRODUCTION

Many modern Army missile systems utilize radomes made of dielectric materials for housing sophisticated electrical instrumentation and guidance components. These radomes are often bonded to the shell of the missile structure using special glue compounds designed to withstand the extreme conditions found in flight. In order that the success of a flight mission be insured it has been found necessary to inspect the glue bond lines in these radomes.

Modern radiographic techniques using x-rays and neutron bombardment are both expensive and often insensitive to the detection of disbonds in the missile structure. It is imperative that a nondestructive technique be developed for rapid low cost testing of these structures.

After much investigation it was found that acoustical testing could adequately serve this testing function and at a minimal cost. This report documents a working system for testing a variety of radome structures using the technique of pulse echo scanning.

Pulse echo scanning may be described as follows in *Figure 1*. In this type of scanning, an ultrasonic transducer operating between 1 and 5 MHz is pulsed with an RF pulse of usually 1-5 μs duration. Depending upon the type and orientation of the transducers, either a longitudinal or shear wave is generated which propagates toward the radome ceramic. When the ultrasonic pulse reaches the ceramic, a portion of it is reflected back toward the transducer, which results in a front surface echo return, and the remainder propagates toward the glue bond line. If a good glue bond is present the transmitted ultrasound will be attenuated. Conversely, if a poor bond is present an echo will be reflected from the ceramic-fiberglass bond line toward the transmitting transducer. By examining the amplitude of the echo return from the glue bond line, one can determine the quality of the glue bond (*Figure 2*).

The major problems encountered in pulse echo scanning are the interpretation of the return echo amplitudes and the provision of sufficient electrical gating sensitivity and detectability of the return echos. This report documents a system for scanning radome glue bond joints such as found in the Pershing II and PATRIOT missile systems. Section 2 gives the mathematical analysis and terminology necessary for glue bond analysis while Section 3 describes the operation of the system and gives pertinent electrical information. Experimental scanning techniques and results are given in Section 4 while Section 5 documents general conclusions which can be made about the system. The Appendix contains a full description of the computer codes necessary for the operation of the system in computer mode.

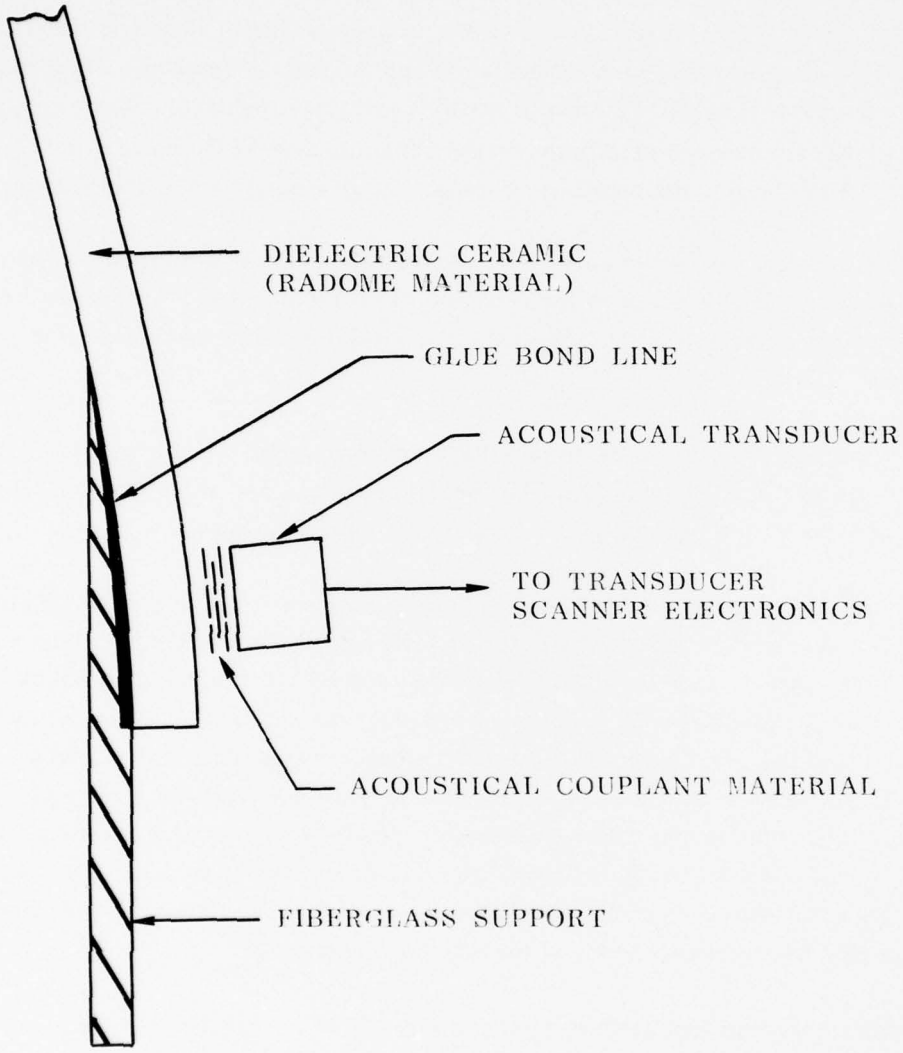

Figure 1. Basic transducer geometry.

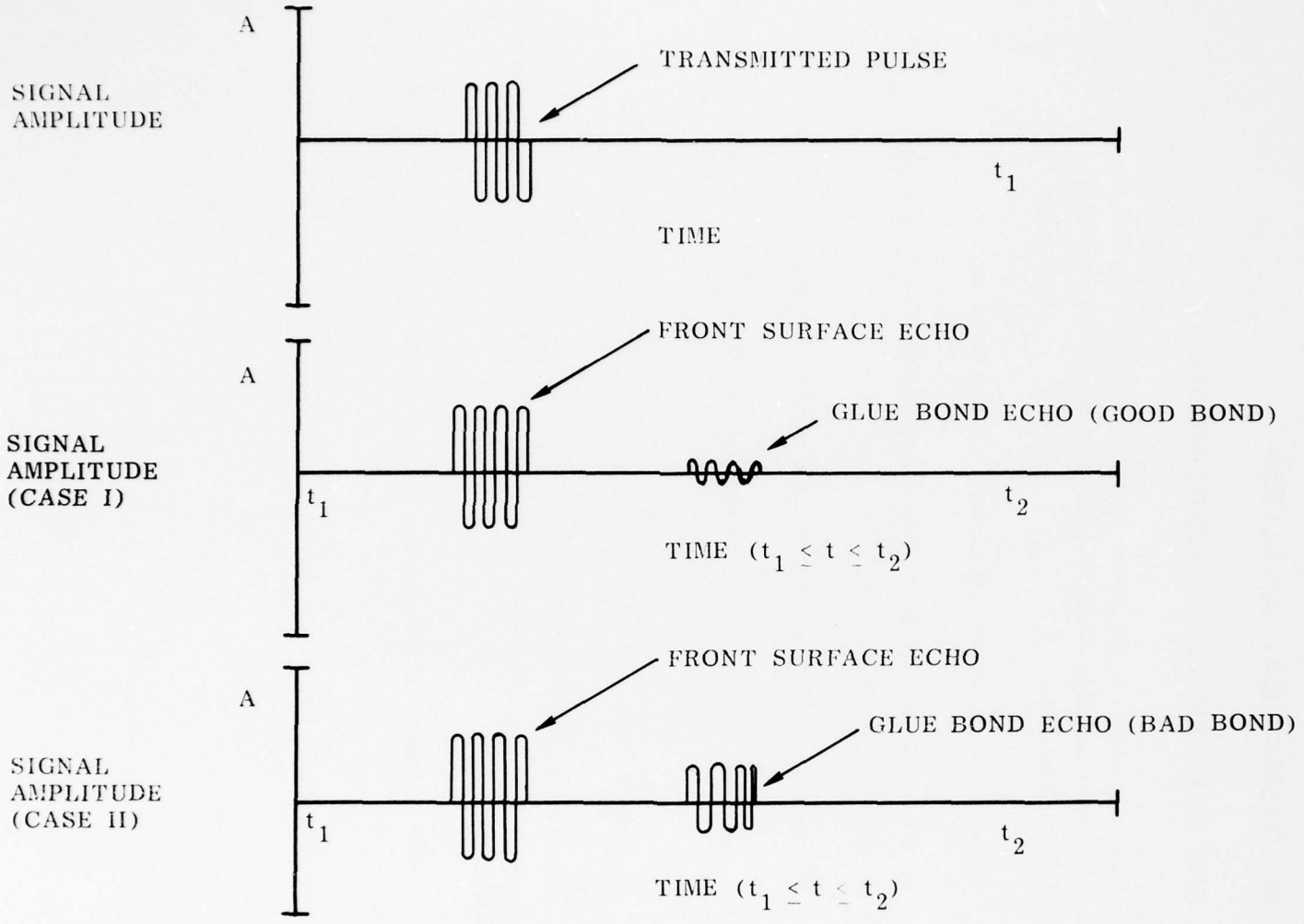

Figure 2. Comparison of echo returns characterizing glue bond integrity.

2. MATHEMATICAL ANALYSIS

A. ONE DIMENSIONAL ACOUSTIC MODEL

In order to characterize the nature of a glue disbond a physical description of the insonification process will be developed. Consider *Figure 3* which depicts the process. Define the following parameters:

I $\equiv$ incident energy on the ceramic front surface (Joules/cm^2 etc.)

ρ_A $\equiv$ front surface reflectivity (1 = perfect reflector) of ultrasonic passing from external media to ceramic

ρ_B $\equiv$ rear surface reflectivity of ultrasound passing from ceramic to external media

K $\equiv$ acoustical couplant attenuation constant from the transducer to the ceramic front surface (0 = perfect attenuation)

ϵ $\equiv$ ceramic attenuation constant from the front to the rear ceramic surface.

It is important to note that K and ϵ depend upon the materials and their geometry. Furthermore, it is assumed that ρ_A and ρ_B are dependent on the direction of propagation of the ultrasound.

With these definitions the anticipated echo-return energy densities may be shown to be as follows:

Front surface reflection

$$I_{R0} = K\rho_A I \tag{1}$$

First glue bond reflection

$$I_{R1} = K\epsilon^2(1-\rho_A)I\rho_B(1-\rho_B) \tag{2}$$

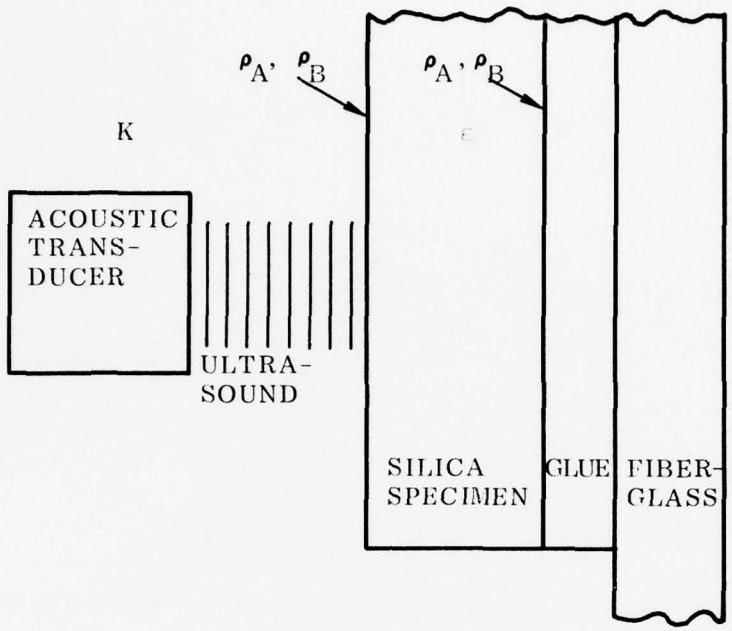

Figure 3. Insonification model.

Second glue bond reflection

$$I_{R2} = K\varepsilon^4(1-\rho_A)I\rho_B{}^3(1-\rho_B) \tag{3}$$

Third glue bond reflection

$$I_{R3} = K\varepsilon^6(1-\rho_A)I\rho_B{}^5(1-\rho_B) \tag{4}$$

Fourth glue bond reflection

$$I_{R4} = K\rho^8(1-\rho_A)I\rho_B{}^7(1-\rho_B) \tag{5}$$

Then the following equations exist:

$$\varepsilon\rho_B\Big|_a = \sqrt{\frac{I_{R2}}{I_{R1}}} \quad ; \quad \varepsilon\rho_B\Big|_b = \sqrt{\frac{I_{R3}}{I_{R2}}} \quad ; \quad \varepsilon\rho_B\Big|_c = \sqrt{\frac{I_{R4}}{I_{R3}}} \tag{6}$$

and

$$\frac{I_{R1}}{I_{R0}} = \frac{\varepsilon^2(1-\rho_A)\ \rho_B(1-\rho_B)}{\rho_A} = \phi\rho_B(1-\rho_B) \tag{7}$$

where,

$$\phi = \frac{\varepsilon^2(1-\rho_A)}{\rho_A} .$$

It is important to note that if ϵ and ρ_A are constants then ϕ becomes a material constant.

The model previously described assumes that ultrasound passing from the ceramic to another media always reflects the same; this is not always true. To account for this an improved model is given:

Define:

ρ_A ≡ reflectivity in going from the acoustical couplant to the ceramic

ρ_B ≡ reflectivity in going from the ceramic to the glue

ρ_C ≡ reflectivity in going from the ceramic to the acoustical couplant

I ≡ incident energy density of the ultrasound at the couplant ceramic interface

K ≡ acoustical couplant attenuation constant

ϵ ≡ ceramic attenuation constant.

Therefore, the following equations result:

Reflected pulse from the ceramic front surface

$$I_{R0} = K\rho_A I \tag{8}$$

Ceramic-glue bond reflected pulse

$$I_{R1} = K\varepsilon^2(1-\rho_A)I\rho_B(1-\rho_C) \tag{9}$$

Then,

$$\frac{I_{R1}}{I_{R0}} = \frac{K\varepsilon^2(1-\rho_A)I\rho_B(1-\rho_C)}{K\rho_A I} \tag{10}$$

or

$$\eta = \frac{I_{R1}}{I_{R0}} = \Phi\rho_B \tag{11}$$

where $\Phi = \dfrac{\varepsilon^2(1-\rho_A)(1-\rho_C)}{\rho_A}$ a material constant.

Now, if it is assumed that I_{R1} and I_{R0} are proportional to the rear and front surface echo return amplitudes respectively, then their ratio characterizes the glue bond reflectivity. It is anticipated that η will approach one if a glue disbond is present since I_{R1} will have increased in magnitude.

B. TRANSMISSION AND REFLECTION FROM LIQUID-SOLID BOUNDARIES

The expressions for analysis of the propagation of vibrational pulses through layered media will be stated here without derivation. For a more detailed discussion of these expressions, the reader is referred to L. M. Brekhovskikh [1].

Consider an acoustic wave of the form

$$p_{inc} = p_1 + \cos(wt-Kz) \tag{12}$$

normally incident on the boundary between medium 1 ($Z_1 = \rho_1 C_1$) and medium 2 ($Z_2 = \rho_2 C_2$) - *Figure 4*.

For this case:

$C_i \equiv$ velocity of propagation in media i

$\rho_i \equiv$ density of media i

$Z_i \equiv$ characteristic impedance of media (i).

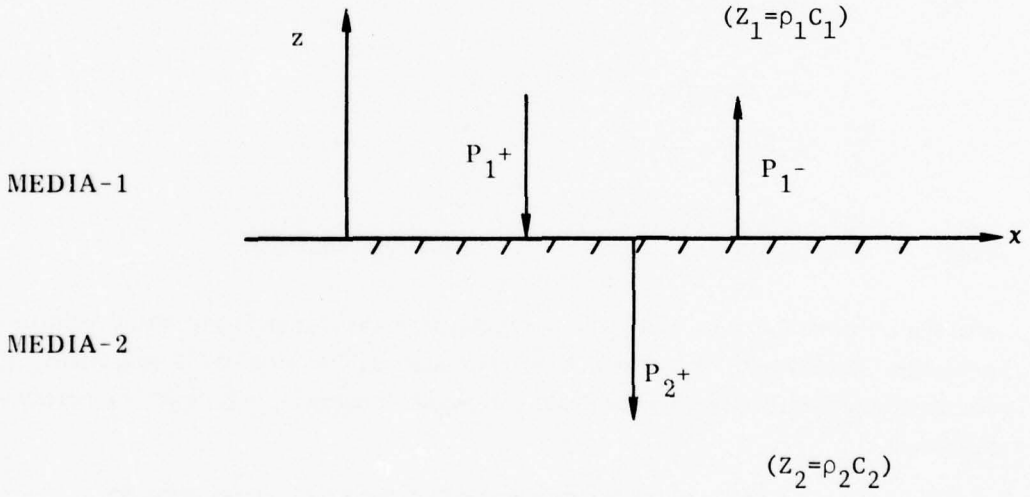

Figure 4. Geometry for calculation of pressure reflection and transmission coefficients at normal incidence.

The pressure reflection coefficient can then be written in the form:

$$V_{12} = \frac{P_1^-}{P_1^+} = \frac{Z_2-Z_1}{Z_2+Z_1} \tag{13}$$

and the reflected wave can be expressed as

$$\text{Pref} = P_1+V_{12}\cos(wt-kz) \quad . \tag{14}$$

The refracted wave can be written in the form:

$$\text{Ptravs} = W_{12}P_1+\cos(wt-kz) \tag{15}$$

where

$$W_{12} = \frac{2Z_2}{Z_1+Z_2} = \frac{P_2^+}{P_1^+} \quad . \tag{16}$$

As has been shown previously, an important parameter in ceramic radome studies is the ratio of the echo from the front surface of the radome (water-ceramic interface) to the echo from the ceramic-glue interface. The geometry of this process for a slip-cast fused silica-ceramic radome is shown in *Figure 5*. This results in the expression:

$$\eta = \frac{W_1^-P_2^-}{V_1^+P_1^+} \quad . \tag{17}$$

The importance of such a ratio is that it primarily eliminates to a first order approximation effects of transducer nonuniformity. In terms of the acoustic impedances of the materials involved, given in *Table 1*, the ratio between the silica-water and silica-glue echoes can be written as:

$$R = \frac{P \text{ glue reflection}}{P_1^+V_1^+} = \frac{4Z_1Z_2(Z_3-Z_2)}{(Z_2^2-Z_1^2)(Z_3+Z_2)} \quad . \tag{18}$$

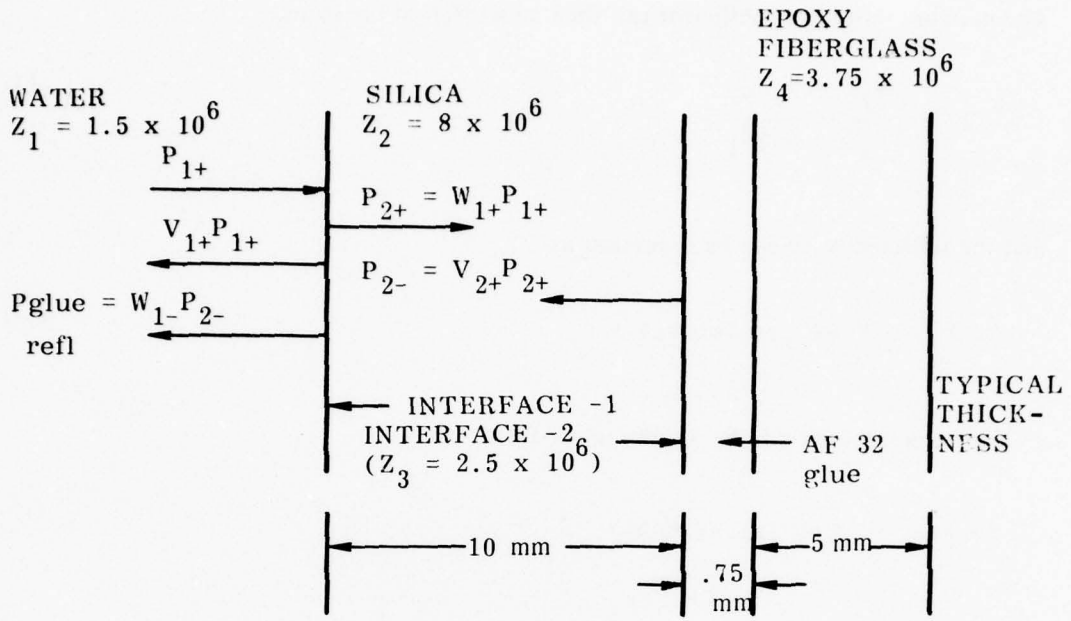

Figure 5. Geometry for calculation of the ratio of the glue reflection to the water-silica reflection Pglue/V_1+ P_1+.
refl

In terms of the reflection and transmission coefficients, the ratio can be written as:

$$R = \frac{W_{12}W_{21}V_{21}}{V_{12}} \tag{19}$$

where for example W_{12} is the transmission coefficient for a wave approaching interface 1 in the positive direction. Using the impedances in *Table 1*, the computed value of R = -.38, assuming no ultrasound beam spreading, absorption or angle effects.

Generally the effects of the various interfaces can be considered separately in the pulsed scanning case since the pulse exists only in a constrained region of space and time. This is not necessarily true in the case of the glue layer since the nominal thickness is about one acoustical wavelength and the typical pulses are several wavelengths long. Thus interference between the front and back surface echoes could cause a diminution in the echo from a good glue joint.

Taking into account the various interface effects, the theory predicts as much as a 28% diminution of the reflected pulse from the silica-glue interface.

TABLE 1. ACOUSTICAL VELOCITIES, DENSITIES AND IMPEDANCES FOR MATERIALS OF INTEREST.

MATERIAL	DENSITY ρ Kg/m^3	ACOUSTICAL VELOCITY LONGITUDINAL (c) m/s	ACOUSTICAL VELOCITY SHEAR (b) m/s	CHARACTERISTIC IMPEDANCE ($Z=\rho c$) LONGITUDINAL	CHARACTERISTIC IMPEDANCE ($Z=\rho b$) SHEAR
WATER	1×10^3	1.5×10^3	NONE	1.5×10^6	NONE
IMPREGNATED SILICA*	1.96×10^3	4.08×10^3	2.5×10^3	8.00×10^6	4.9×10^6
GLUE (AF32)	1.25×10^3	2.0×10^3	---	2.5×10^6	---
EPOXY FIBERGLASS	1.5×10^3	2.5×10^3	---	3.75×10^6	---
FUSED QUARTZ	2.20×10^3	5.95×10^3	3.75×10^3	13.09×10^6	8.25×10^6

*Acoustical velocity and density of silica varies widely depending on its preparation.

C. TRANSMISSION AND REFLECTION AT OBLIQUE (NON-NORMAL) INCIDENCE

The first interface in the system is the water-silica interface. The pressure reflection coefficient as a function of incident angle of a wave traveling from a liquid medium into a solid at an angle below the critical angle is

$$V_{12} = \frac{P_{1-}}{P_{1+}} = \frac{Z_2\cos^2 2\gamma_2 + Z_{2t}\sin^2 2\gamma_2 - Z_1}{Z_2\cos^2 2\gamma_2 + Z_{2t}\sin^2 2\gamma_2 + Z_1} \tag{20}$$

where the geometry is as shown in *Figure 6*, $Z_1 = \rho_1 C_1 / \cos\theta_1$, $Z_2 = \rho_2 C_2 / \cos\theta_2$, $Z_{2t} = \rho_2 b_2 / \cos\gamma_2$ and b_2 is the velocity of the transverse wave in medium 2. To evaluate this expression it is also necessary to use Snell's law,

$$\frac{\sin\theta_1}{C_1} = \frac{\sin\theta_2}{C_2} = \frac{\sin\gamma_2}{b_2} . \tag{21}$$

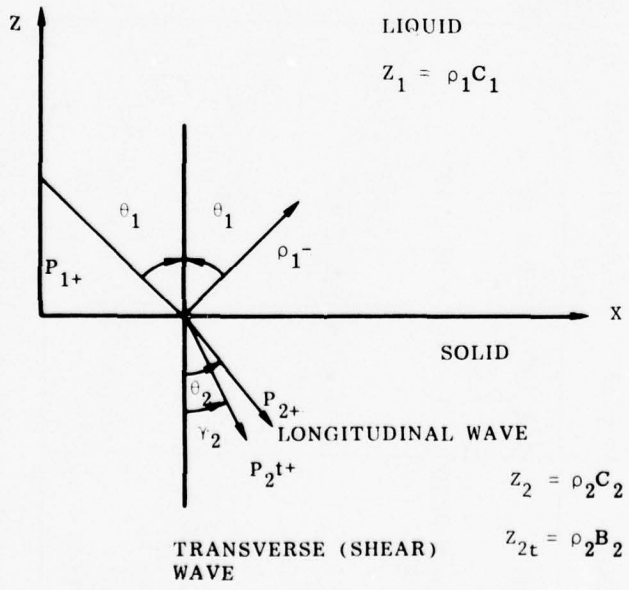

Figure 6. Geometry for calculation of reflection and transmission coefficients at oblique incidence to a liquid-solid interface.

The longitudinal wave transmission coefficient is

$$W_{12} = \frac{2Z_2\cos 2\gamma_2}{Z_2\cos^2 2\gamma_2 + Z_{2t}\sin^2 2\gamma_2 + Z_1} = \frac{P_{2+}}{P_{1+}} \tag{22}$$

and the shear wave transmission coefficient is

$$P_{12} = \frac{P_{2t+}}{P_{1+}} = \frac{2Z_{2t}\cos 2\gamma_2}{Z_2\cos^2 2\gamma_2 + Z_{2t}\sin^2 2\gamma_2 + Z_1} \tag{23}$$

Using the values of *Table 1*, the calculated magnitude of the reflection coefficient as a function of angle for the silica-water interface is shown in *Figure 7*. It should be noted that for an incident angle of less than 20° the reflection coefficient changes less than 3.5% from the value at normal incidence. At $\theta_{c\ell}$, the critical angle for longitudinal wave propagation, the reflection coefficient peaks very sharply to unity and then drops to within 13.5% of the value at normal incidence from 22° to 36°. Beyond $\theta_{ct} = 36.87°$, the critical angle for transverse or shear waves, the magnitude of the reflection coefficient is unity. It should be noted that the phase of the reflection coefficient will vary for $\theta_1 > \theta_{c\ell}$ (phase = 0 for $\theta_1 < \theta_{c\ell}$) but here one is primarily interested in the magnitude of the reflection coefficient.

Figure 8 shows a ray trace of the beam from a transmitting transducer at the very top of the bond line. Here the angle of the glue joint with respect to the front surface of the silica is greatest. Note that the main lobe of the reflected beam entirely misses the receiving transducer, which will be in the sidelobe region.

Overall, the results of these calculations indicate that oblique incidence effects should not appreciably alter the magnitude or phase of the beam from the values obtained at normal incidence. The geometry of the radome joint is such, however, that the bond line echo strength can be reduced considerably due to the curvature at the bondline.

3. SYSTEM DESCRIPTION AND OPERATION

The acoustical array signal processor (SNDT-1000) was built for the Ground Equipment and Missile Structures Directorate by Sperry Support Services. The device is a stand-alone unit with optional computer interfacing available. The unit consists of the following sub-units:

- Model SNDT-1000 signal processor

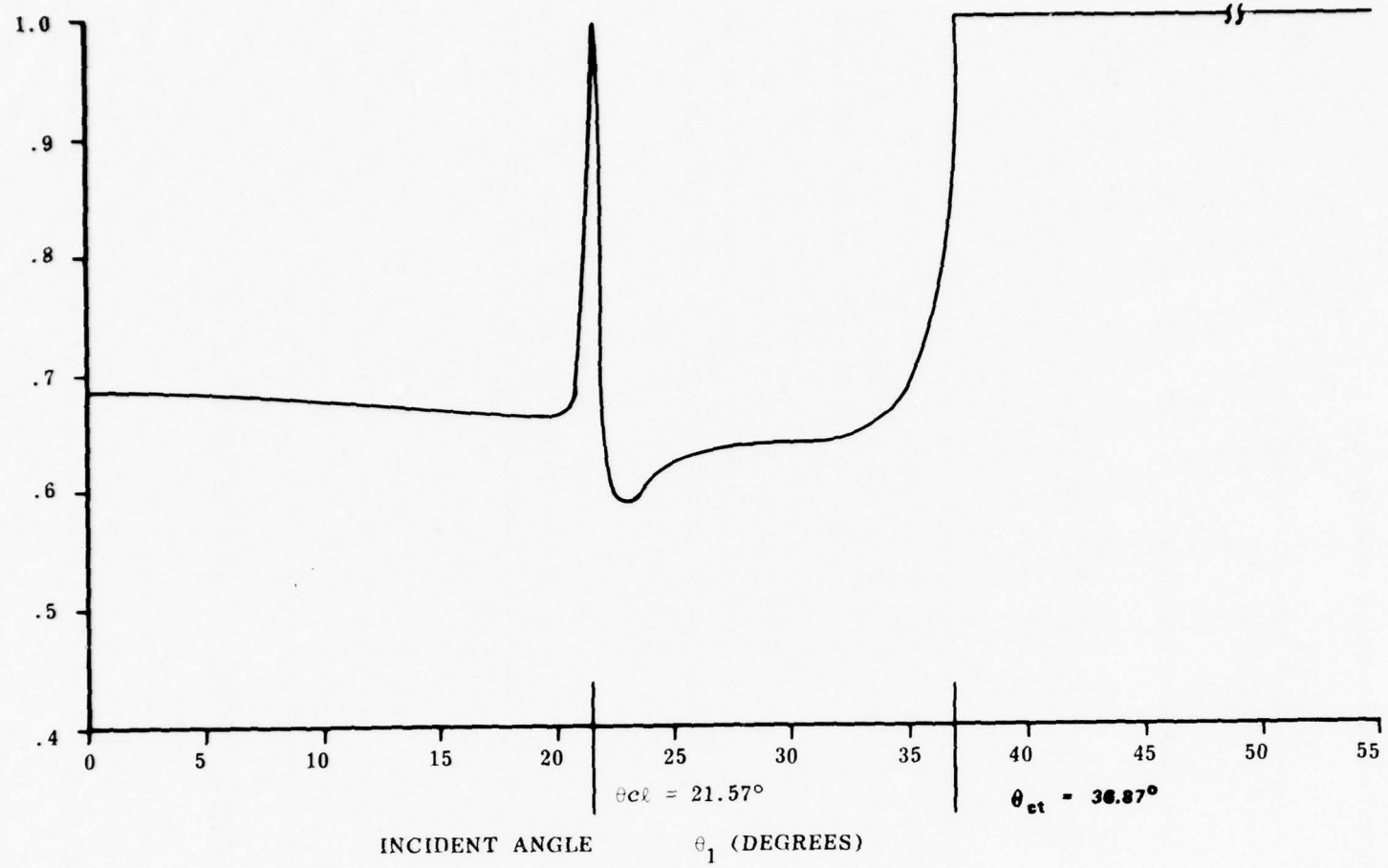

Figure 7. Theoretical magnitude of the reflection coefficient |V| as a function of incident angle, for a silica-water interface using Equation (20) and the values contained in Table 1.

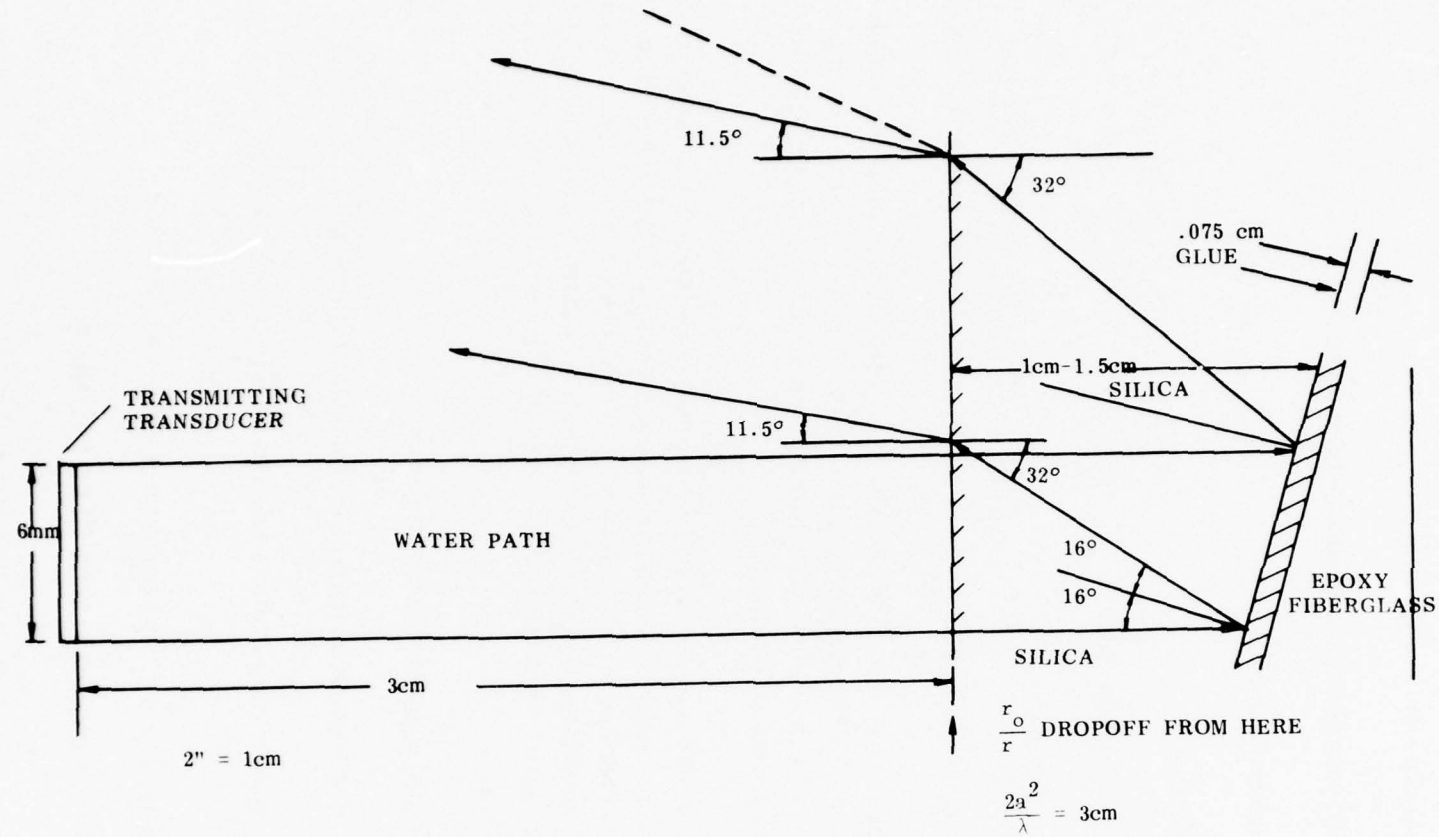

Figure 8. Ray trace of beam envelope from transmitting transducer, through silica, and back to transducer. Worse case conditions.

- Preamplifier and array system
- Digital controlled rotating table and controller.

Optional accessories are:

- Oscilloscope
- XY video storage scope
- Scan controller
- External power amplifier.

The system features 14—.25 × .25 inches 2.25 MHz Dapco transducers which can scan approximately 434,000 different locations on the glue bond line of a Pershing II radome. *Figure 9* shows the basic components of the system. References [2] and [3] should be consulted for detailed operating instructions.

The SNDT-1000 operates using a dual transmit/receive multiplexed transducer system. In this system 14 transducers are sequentially keyed with a 2.25 MHz RF sine wave. The ultrasound propagates toward the test piece (radome) which then reflects the ultrasound back toward the transmitting transducer which is then switched into a receiver mode. The received signal from each transducer is then amplified and one of the following operations is performed:

- The signal is displayed on an oscilloscope;
- The signal is sampled and held for computer digitization; or,
- The signal is compared to a reference voltage to turn a storage scopes z-axis beam intensity on or off.

Figures 10 and *11* show block diagrams of the system electronics.

A. SYSTEM COMPONENT ELECTRONICS

The information available to the computer is:

(a)

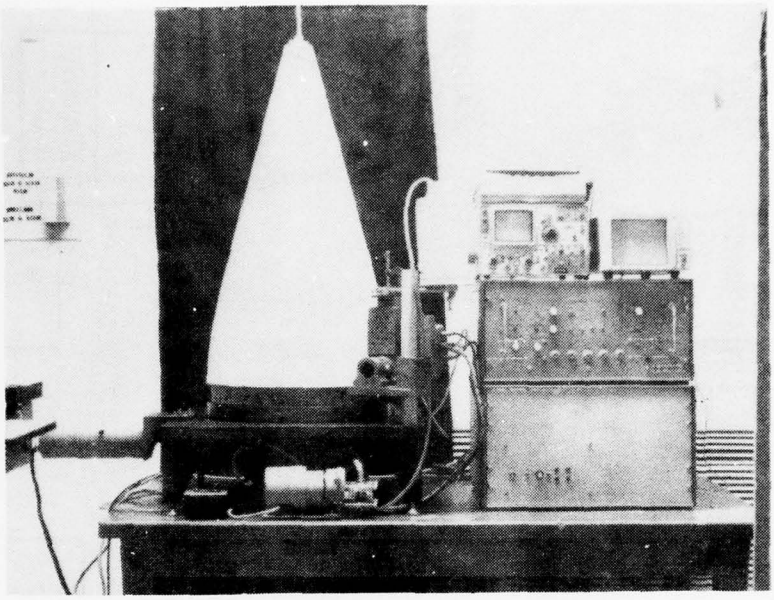

(b)

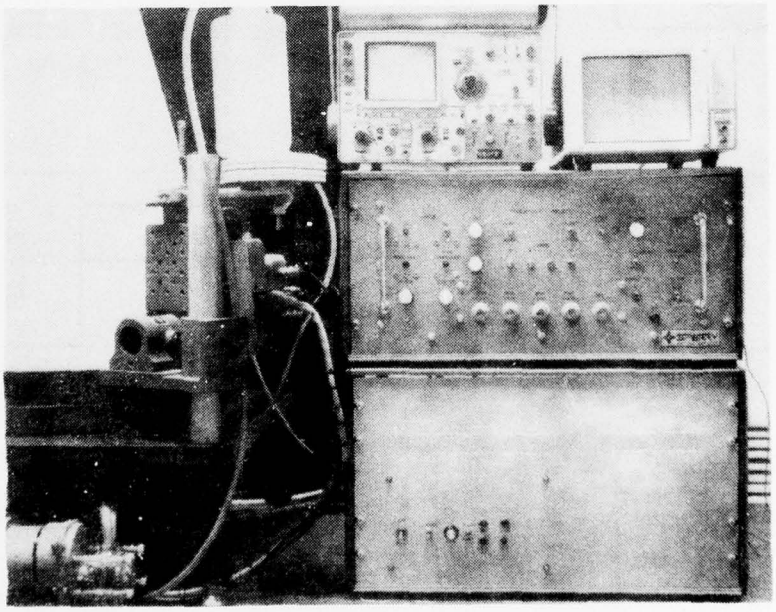

Figure 9. Array signal processor unit. (a) Entire system scanning Pershing II radome. (b) Close-up view of control electronics.

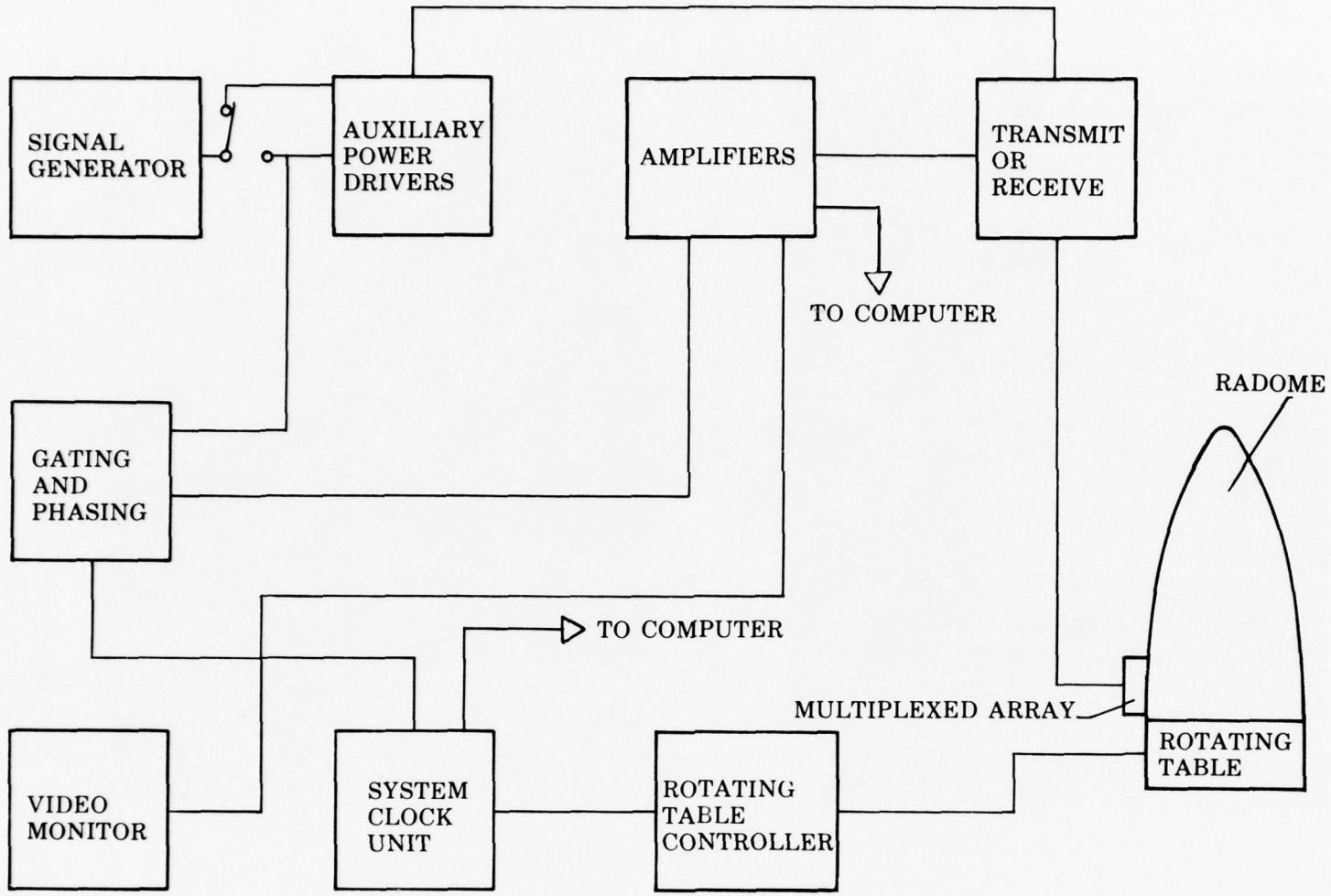

Figure 10. Acoustical Array Scanner system block diagram.

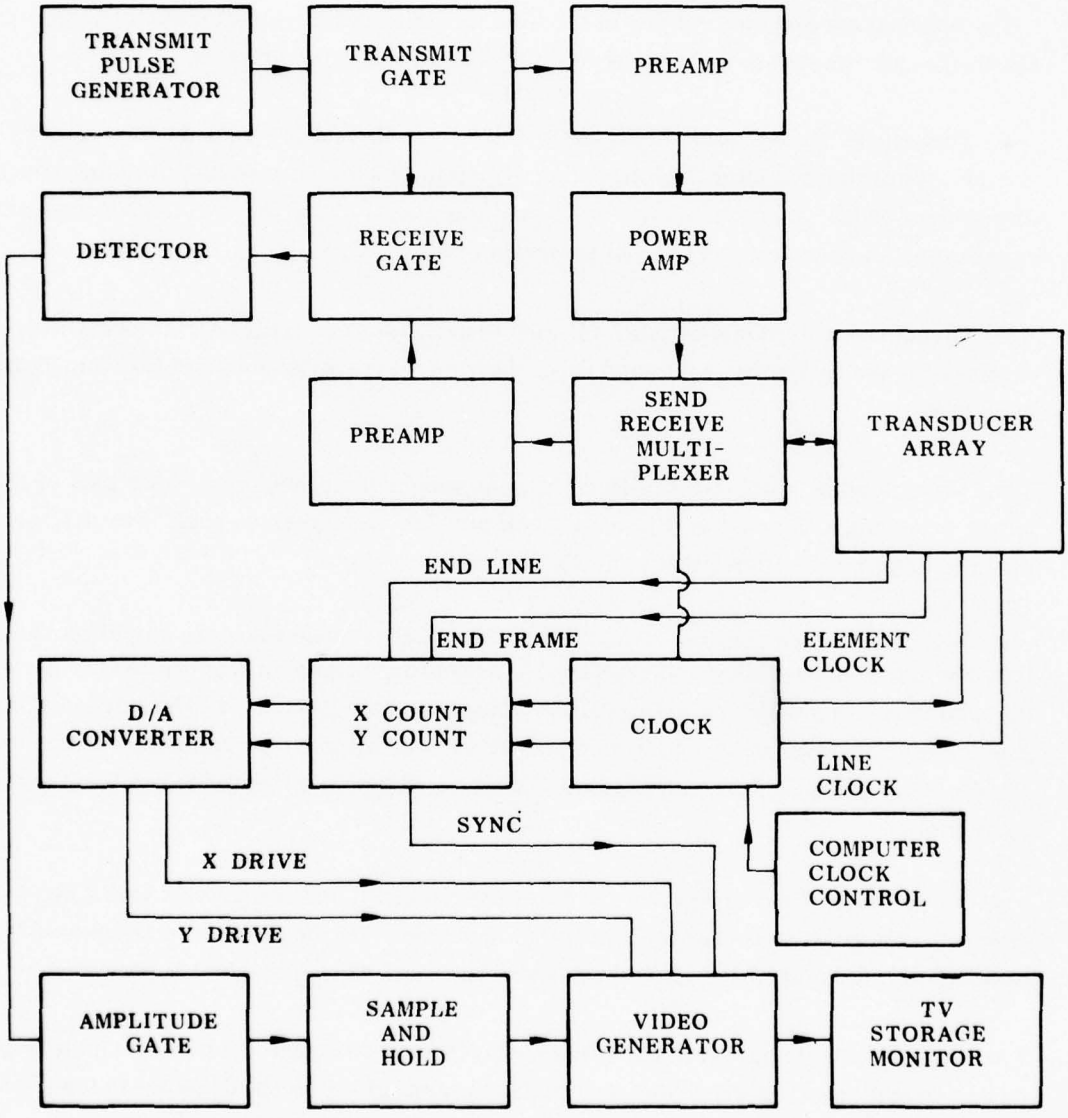

Figure 11. Signal processor and array block diagram.

- x and y position on the radome of each transducer (digital)

- Amplitude of return echo (analog)

- System clock (digital).

The system clock and motor drive for the rotating table can be controlled by the computer. Electronics for the system are mounted on cards and feature the following:

- Transducer Exciter and Power Amp Card—this circuit provides an internal VFO (variable frequency oscillator) and the gating circuits to develop a transmit pulse of the proper timing and width. It also contains a 15 db amplifier for driving the transducers and connections for an external VFO and power amplifier.

- Clock, Drive, and Gate Generator Card—this circuit contains the system clock with rate controls and the gate delay, width and drive electronics for sample and hold scanning of the return echo.

- Video Clipper Card—this circuit has an amplifier for providing a 40 db gain of the return echo with clipping of the echo at about 2.4 volts peak-to-peak. The RF gain potentiometer on the front panel controls this card.

- Signal Gate Detector and Sample/Hold Card—this circuit takes the amplified signal from the video clipper circuit and gates it with the gate drive signal to produce an envelope of the echo. The Sample/Hold gives a level representation of the echo on the rising portion of the gate pulse. This level is sent to a comparator card or an external computer. When the Sample/Hold switch is in the out position, the echo envelop itself is amplified and sent to the comparator.

- Comparator Card—this circuit receives the echo level and compares it with a positive reference voltage. A level change from low to high represents the presence of an echo from a disbond. A bond fault light on the front panel turns off when a disbond is present.

- Array Control and Sweep Generator Card—this card controls the position of the beam on a storage monitor for displaying the results of scanning the glue bond line of a radome. The master reset button on the front panel resets all sweeps back to 0.

- Transducer Selector Card—manual selection of transducer for display purposes or their

automatic sequential operation is controlled by this card. A control switch on the front panel selects the mode of operation and four switches sequence the transducers manually.

- Transducer Array Card—this circuit features FET switches used to turn on each of the 14 transducers.

- Line Driver Card—computer interfacing is provided by this card which provides six lines of binary coding for the angular orientation of the radome to the array and six lines for the y axis (height) of the transducer on the radome. The motor drive logic and signal conditioner for the rotating table are also on this card. An adder circuit is also present which combines the Sample and Hold signal with the clock pulse and a line driver to provide echo information to a computer for data reduction.

B. THEORY OF OPERATION

The scanner system operates as follows. A 1-3 MH$_z$ sine wave oscillator output from a VFO is gated to produce a transmit pulse. This transmit pulse is amplified and the attenuation control is provided by an RF drive potentiometer on the front panel. The transmit pulse is either sent to a single transducer (manual mode) selected on the front panel or sequentially sent to each of the 14 transducers. After each transducer is pulsed with the RF signal, they are switched to receiver mode. In this mode the entire return echo from the test object is amplified and a portion of this echo is gated to a Sample/Hold—comparator circuit. If the system is in Sample and Hold mode the rising edge of a gate pulse activates a Sample and Hold circuit which samples the echo over about a 20 ns time interval. The amplitude sampled is then sent to a computer or displayed on a scope. If the system is in comparator mode, the Sample and Hold signal or the envelope of the echo signal is compared to a reference voltage. If the envelope or Sample/Hold signal goes above the reference level, a disbond is present. The presence of a disbond turns off the bond fault indicator light on the front panel and also blanks the z intensity pulse for writing to the video monitor thus indicating the presence of the flaw. *Figure 12* shows the layout of the front panel controls for scanning purposes. After each set of 14 transducer scans of the glue-bond line are made the radome is incremented approximately $2\pi/1024$ radians and a new scan is made. If a computer is used to control scanning, increments of $2\pi/31000$ radians are possible. When the radome is incremented the X·Y sweep of the video monitor displaying the disbond is also incremented.

C. OPERATING CONTROL FUNCTIONS

The following control functions are available on the front panel of the scanner unit.

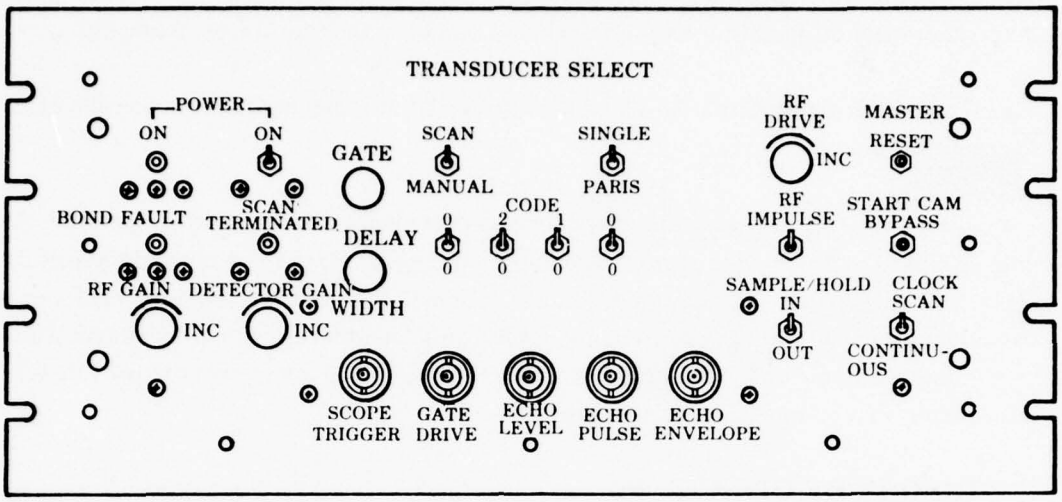

Figure 12. Front panel of Array Signal Processor.

1. RF Drive: Sets the transmit level voltage to the transducers.

2. RF Gain: Sets the amplification level to the video amplifier of the return echo.

3. Detector Gain: Sets the amplification of the DC amplifier.

4. Power: Turns the system on. A red LED beside this control indicates system operation.

5. Excitation: This control determines if a keyed RF signal or a square wave transmit pulse is applied to the transducers in the array.

6. Sample/Hold: When placed in the IN position a DC level representation of the detected echo on the rising portion of the gate pulse is given. When in the OUT position this circuit is bypassed. The circuits output may be observed on the Echo Pulse BNC connector on the front panel.

7. Master Reset: This switch resets the X-Y position of the video monitor and transducer select to 0.

8. Start Cam Bypass: A single scan of 14 transducers is made.

9. Clock: The transducers are continuously scanned.

10. Bond Fault: Indicates the presence of a glue disbond on an LED which turns off in its presence.

11. Scan Terminated: This LED is activated when the scanning process has stopped.

12. Gate Delay: Positions the signal gate from 10 ns to 10 ms.

13. Gate Width: Sets the width of the gate from 50 ns to 5 ms.

On the back panel of the system a switch is present which allows a computer to control the position of the gate.

4. EXPERIMENTAL SCANNING TECHNIQUES AND RESULTS

A number of experimental procedures were carried out in support of the array design and application. These procedures included measurements of transducer impedances and field patterns at various frequencies and scans of bond lines of both test samples with programmed flaws and two actual radomes. The overall results were indicative that the system has the ability to detect both flaws in silica and in the silica glue bond line. Some problems in flaw detection in the bond line of actual radomes were identified in the testing program and means for overcoming these problems are suggested.

A. TRANSMISSION STUDIES

Given the impedances of *Table 1*, the expected pressure transmission coefficient for the composite radome base is about .7. The geometry for this calculation is shown in *Figure 13*. In general, the measured transmission coefficients were less than .1, suggesting an additional source of attenuation. The low transmission coefficients appear to be primarily due to the large number of air bubbles in the glue joint of the Pershing II radome first studied. This is further indicated by the neutron radiograph shown in *Figure 14*.

The procedure for taking transmission readings was as follows: (1) a pincers transducer holder was devised to hold the two transducers in approximate face-to-face orientation on

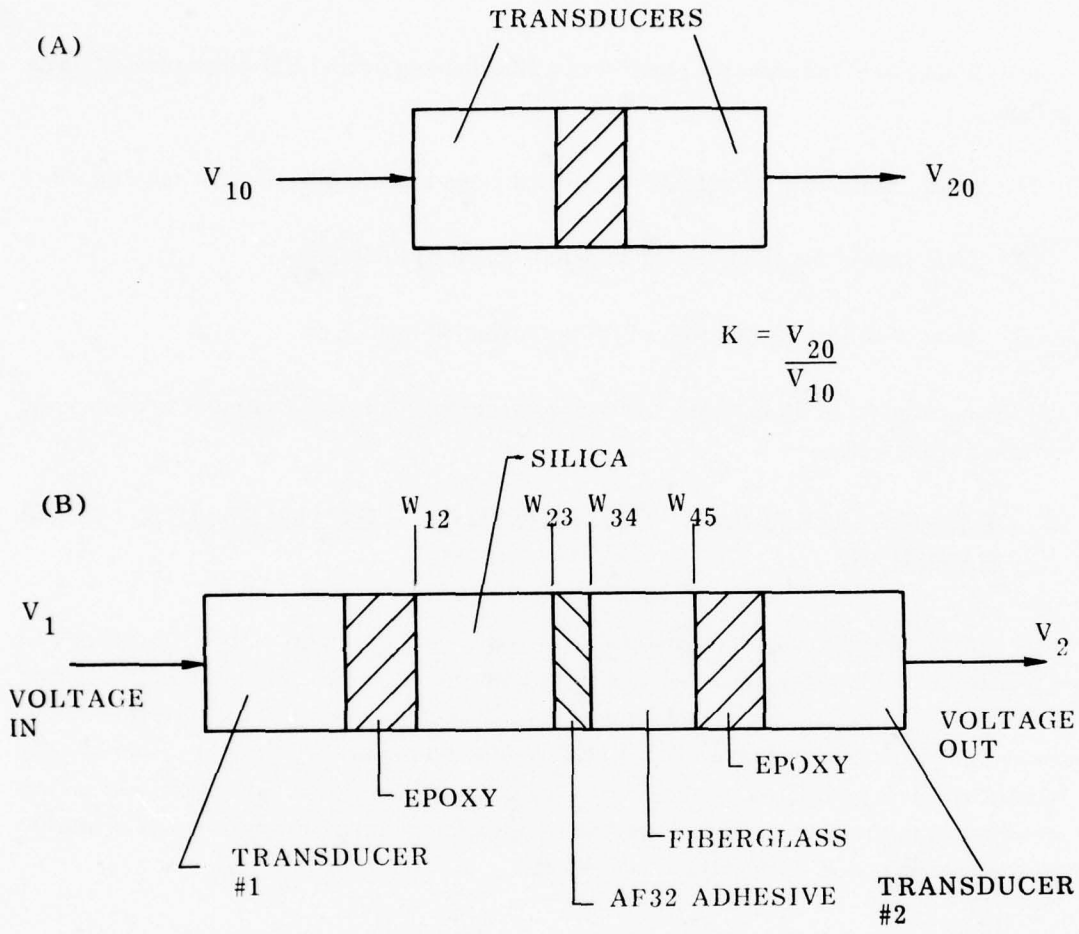

Figure 13. Geometry for calculation of the ratio (V_2/V_1) of the transmission with a radome inserted between two ultrasound transducers. K is a constant of the transducers, and the impedance of the adhesive layers which are bonded to the transducer faces.

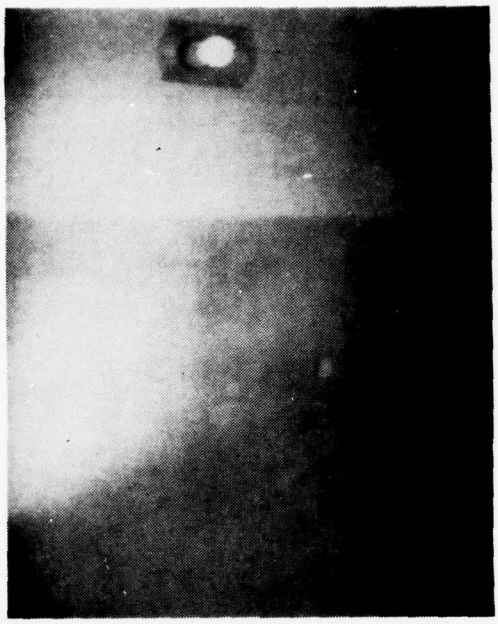

Figure 14. Typical section of neutron radiograph of Pershing II radome under inspection. Note the highly marbled texture in the joint region.

both sides of the radome. This transducer holder is shown in *Figure 15*. (2) after orienting the transducers at a particular level on the radome, minute adjustments in transducer orientation were carried out until the maximum signal was observed. (3) the ratio of the received signal through the radome to the received signal with the two transducers pressed together was taken to be the transmission coefficient for the radome at that point. Results of transmission studies at two relatively high transmission spots on the radome are shown in *Figure 16*. In general, the high transmission regions, which should correspond to the most solid glue regions, were located in the upper half of the bond region.

B. ECHO STUDIES

Due to the very low transmission, obtained through the joint region of radomes, the requirement for access to both sides of the radome, and the poor differentiation between flaw and surroundings obtainable in the transmission mode, the flaw detection system was designed for use in the pulse echo mode. In the pulse echo mode an ultrasonic pulse is sent into the specimen and the echoes from various interfaces are picked up by a receiver, usually the same transmit transducer. The depth of interfaces or flaws in the material can be accurately determined with knowledge of the echo delay and the velocity of sound in the material. Flaws

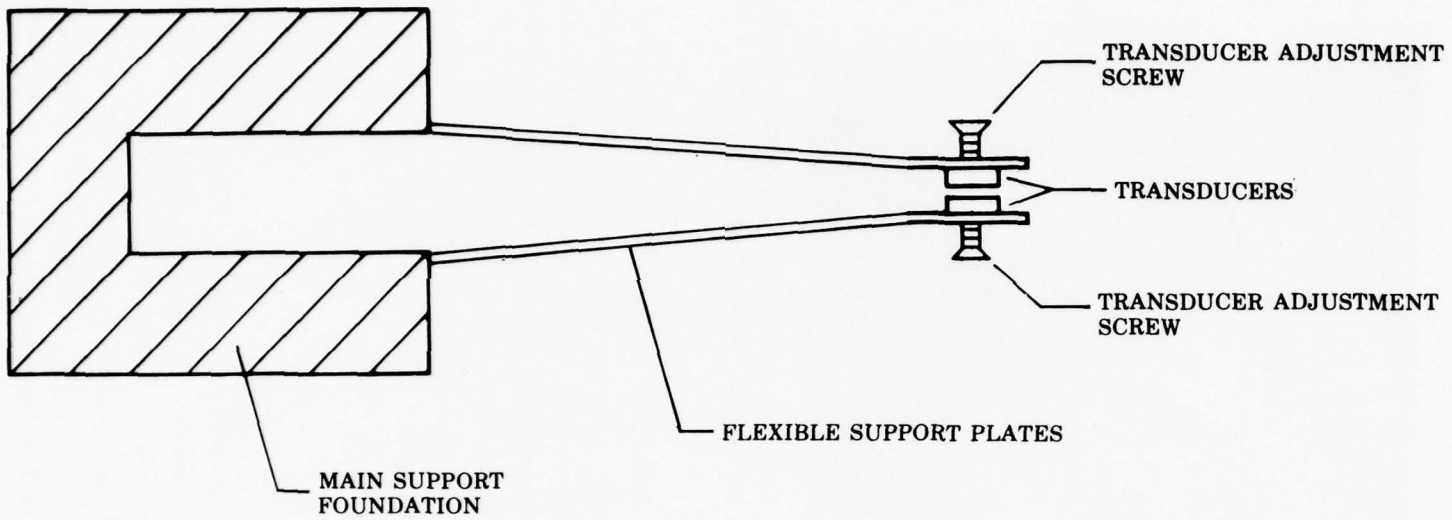

Figure 15. Transducer holder for obtaining ultrasonic transmission measurements on radomes. In actual operation the two transducers were finely adjusted once in position to give the maximum transmission reading used in calculating the transmission coefficient.

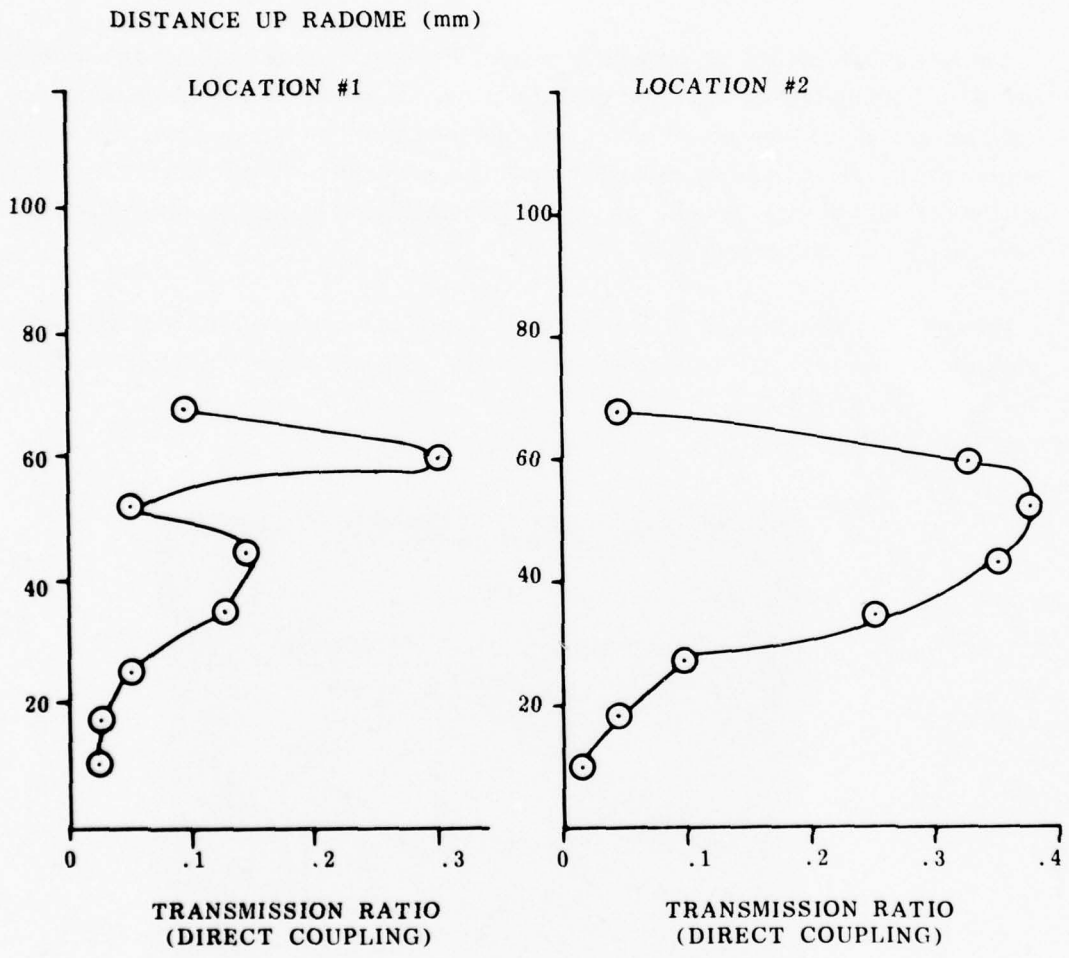

Figure 16. Transmission coefficients as a function of height on the bond line for two locations on Radome Number 1.

or disbonds change the impedance characteristics of the interface and thus can change the echo amplitude or character.

In order to ascertain the expected echo return from various types of flaws, intentional flaws were programmed into a sample of silica-glue-fiberglass material representative of the materials utilized in actual radomes. *Figure 17* shows the three flaws which were produced by boring through the epoxy-glue-fiberglass composite.

A mono-tool was used to cut through the composite producing a flat bottomed hole. For the first flaw, nothing further was done so that a perfect disbond existed between the epoxy-fiberglass and glue. In the second hole, a one-eighth-inch drill bit was used to gouge out the bottom of the hole to simulate an irregular inclusion in the silica. Finally, a screwdriver was used in the third hole to carefully remove the glue layer while leaving the silica intact, thus simulating a disbond between silica and glue.

The array was positioned over each of the three flaws in turn and an oscilloscope was used to study the pertinent echoes from the three transducers closest to the flaw. The results are shown in *Figures 18*, *19*, and *20*.

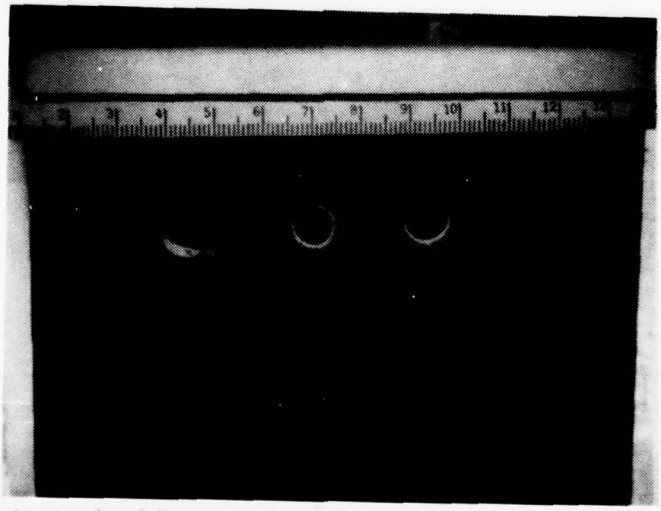

Figure 17. Photograph of flaws manufactured in a test slab using a Dremel Mono-tool with 1/4 inch boring tool. Left to right, flaw in silica, flaw between epoxy-fiberglass and glue, and flaw between silica and glue. The silica flaw was obtained by drilling through silica with a 1/8 inch drill bit, the silica-glue flaw by boring through to glue and cleaning to bare silica.

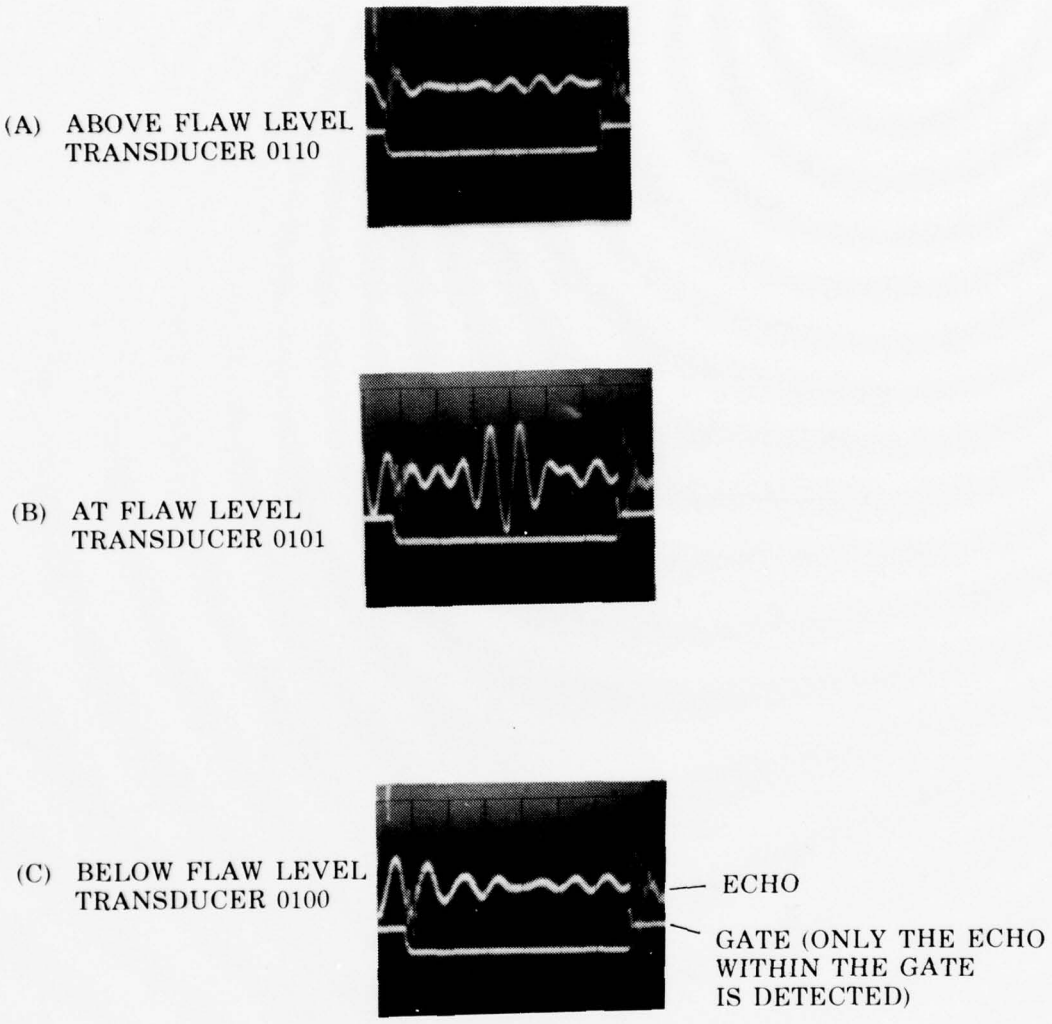

Figure 18. Detection of silica flaw using the ultrasonic array. Echoes above (a), at (b) and below (c) are given for a 9mm diameter programmed flaw. The flaw is about 10 db above reverberations in nonflaw transducer locations.

(A) ABOVE FLAW
TRANSDUCER 0110

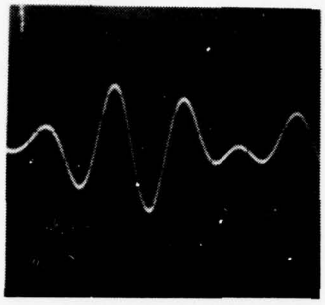

(B) AT FLAW
TRANSDUCER 0101

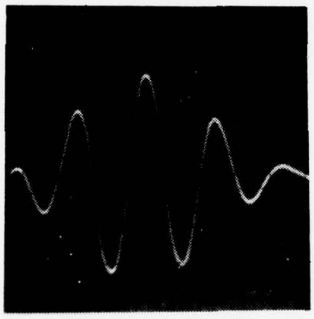

(C) BELOW FLAW
TRANSDUCER 0100

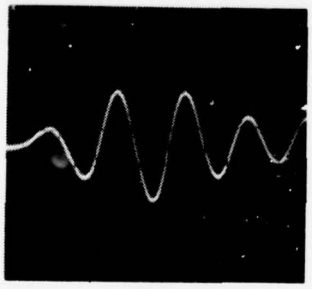

Figure 19. Detection of silica - adhesive bond line flaw. The flaw echo is about 1.8 times the silica adhesive echo (5.1 db and up), which is consistent with the theoretical predicted pressure reflection coefficient for a good adhesive joint of $V_{23} = .5$, since the flaw should give 100% reflection assuming the back surface of the silica is flat.

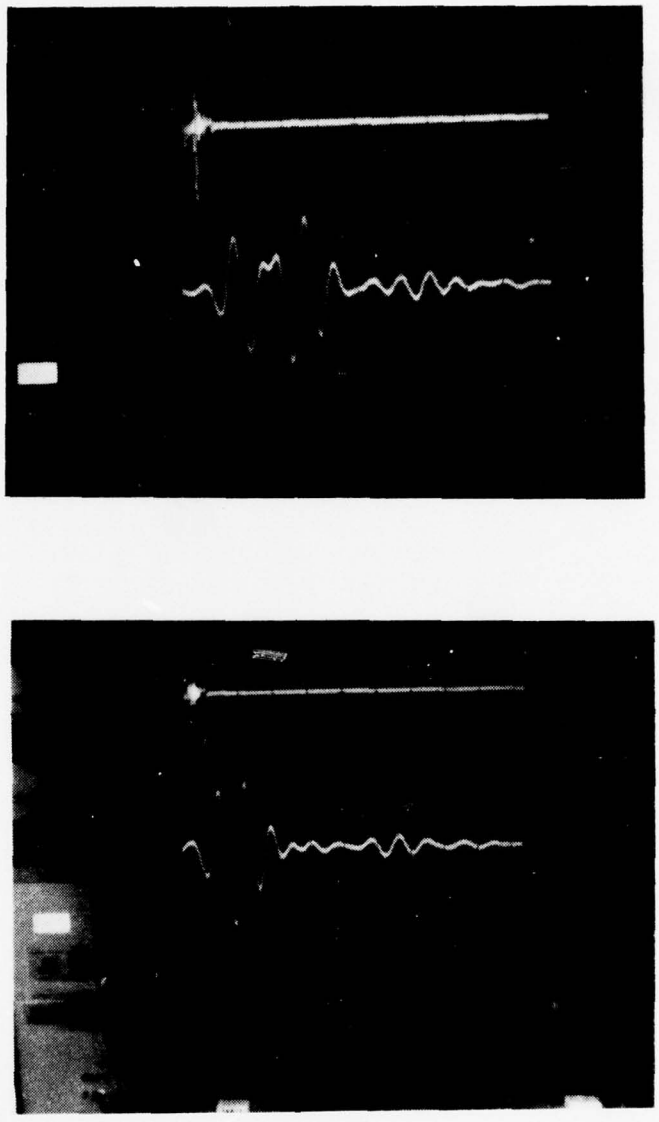

Figure 20. *Echo from (a) over fiberglass-adhesive flaw and (b) from the adjacent point with a good adhesive joint. A single element was used in this experiment. The scope was set on .5 s/cm. Note the phase cancellation in (a) at about .6 ns from onset of pulse; this is about the time predicted for the pulse to travel through the adhesive layer. Note that in (a) the peak-to-peak amplitude of the second portion of the reflection is about 1.3 times the peak-to-peak amplitude of the first pulse. This is predicted by theory.*

The results of these studies show that the array is capable of differentiating three major types of flaws: silica inclusions and cracks, glue-silica flaws and glue-fiberglass flaws. The characteristics of echoes from various types of flaws which can be used to differentiate them are summarized in *Table 2*.

TABLE 2. SUMMARY OF ECHO CHARACTERISTICS TO DIFFERENTIATE MAJOR TYPES OF FLAWS. THE SECOND ECHO :IS THE ECHO APPEARING IMMEDIATELY AFTER THE FRONT SURFACE ECHO FROM THE SILICA WATER INTERFACE.

ECHO CHARACTERISTICS			
FLAW TYPE	SECOND ECHO DELAY TIME FROM ONSET	SECOND ECHO SHAPE	SECOND ECHO AMPLITUDE
SILICA FLAW	ECHO OCCURS SUBSTANTIALLY SOONER	NO CHANGE	DEPENDS ON FLAW ORIENTATION AND SIZE
SILICA-GLUE DISBAND	NO CHANGE	NO CHANGE	INCREASES FROM NORMAL TO A FUNCTION OF TWO AT MOST
EPOXY-GLUE FIBERGLASS DISBAND	NO CHANGE	ECHO IS LENGTHENED. PHASE CANCELLATION APPEARS AT ABOUT .7μS	LITTLE CHANGE; LOBE FOLLOWING SECOND PHASE CANCELLATION MAY BE 40% LARGER

The most important differences between echoes from the various types of flaws are as follows:

- Echoes from silica inclusions and cracks will undergo less signal delay since the structures causing the echoes are closer to the surface of the radome.

- Silica-glue disbond echoes are about twice the amplitude of surrounding echoes from good joints.

- Glue-Epoxy fiberglass disbond echoes are elongated by .6-.7 μsec corresponding to the travel time through the glue layer (AF32 adhesive). Phase cancellation between the echoes from the front and back surface of the glue will be noted at some point in the echo. The second portion of the echo following the phase cancellation should be about 1.4 times the amplitude of the first.

The ratio of the echo from the front surface of the glue layer to the echo from the back surface can be calculated for normal incidence to be

$$\frac{E_{back}}{E_{front}} = \frac{W_{23}\, W_{32}\, W_{34}}{V_{23}} \tag{24}$$

When Equation (24) is evaluated using the impedance values in *Table 1*, and assuming good glue bonds, $E_{back}/E_{front} = .28$. Assuming a disbond between the glue and epoxy-fiberglass, $E_{back}/E_{front} = 1.39$. Thus the effect of a back surface disbond is to produce an echo 40% larger than the front surface echo, with phase reversal, delayed about .7 μsec for a typical glue joint. It should be noted here that echoes were obtained with the transducer aligned directly above the flaw. Studies indicate that alignment is critical and the best results are obtained only with the transducer properly aligned.

In this test one-fourth-inch flaws and one-fourth-inch square transducers were used so that resolution was at the limit of the system. For one-half-inch or larger flaws, alignment should be considerably less critical. The flaws created were idealized for the purpose of evaluating the echo in a controlled situation. In practice, flaws may be hybrid and may exhibit a combination of the characteristics displayed in these experiments. For example, a large flat glue inclusion will give the same general pattern as the glue example flaw except the elongation will be less and the phase reversal will occur earlier.

(1) ACOUSTICAL SCAN TEST NUMBER 1. The following test was conducted to estimate the penetration energy of the acoustic array scanner system. A block of slip-cast fused silica radome material (E modulus≈5-7×10^6psi, ρ≈2gm/cc) was mounted parallel to the 14 transducers. The geometry is as shown in *Figure 21*.

A ruler .079 cm thick with exposed surface area of approximately 1.6 cm^2 was placed on the back surface of the block of silica and coupled acoustically with couplant oil. The ruler was detected everywhere the silica was isonified as it was moved along the back surface of the block. Detection of a good acoustic bond was noted when the reflected pulse off the back surface of the radome decreased by about 50% in amplitude. The transducers were operated at maximum RF and detector gains and their outputs were sequentially monitored on an oscilloscope.

(2) ACOUSTICAL SCAN TEST NUMBER 2. The following test was used to determine the resolution capability of the radome scanning array system. Stainless steel rods were contacted to the back surface of a .65-inch thick piece of slip-cast fused silica using acoustical oil couplant. The transducer selected for resolution studies was number 13, the top unit which appeared to have average amplitude and transmissivity characteristics. The effect of the rod placed on the rear surface is to increase the transmitted energy across the interface boundary—*Figure 22*.

As shown in *Table 3*, the scanner system can detect small areas of disbond and well bonded material fairly well. Full RF and max detector gains were used.

(3) ACOUSTICAL SCAN TEST NUMBER 3. In this test a piece of AF-32 adhesive was bonded to a .5-inch × .8-inch × 6-inch block of slip cast fused silica. Acoustical couplant oil was inserted between the adhesive and a .60-inch thick piece of radome silica which was insonified as in *Figure 23*. A .40-inch square area of silica was insonified. At a simulated bond point, the ultrasound transmissivity increased about 55%. Full RF gain and max detector gain were utilized. The adhesive was bonded for 10 minutes at 300°C temperature minimum.

(4) ACOUSTICAL SCANNER TEST NUMBER 4. The purpose of this test was to evaluate the ability of the array scanner system to detect the bond line quality between pieces of slip-cast fused silica using AF-32 adhesive glue. *Figure 24* shows the geometry used in this test. The AF-32 adhesive was cured using a c-clamp for generating pressure for 30 minutes at a minimum temperature of 300°C. The .588-inch thick silica block was .75-inch wide.

In this test the peak amplitudes of the front and back surface echoes were recorded for the .4428-inch thick silica. Transducers 7-13 have the standard perfect flaw indicated by no silica or glue present at the back of the test block. However, transducers 0-6 have the simulated lab

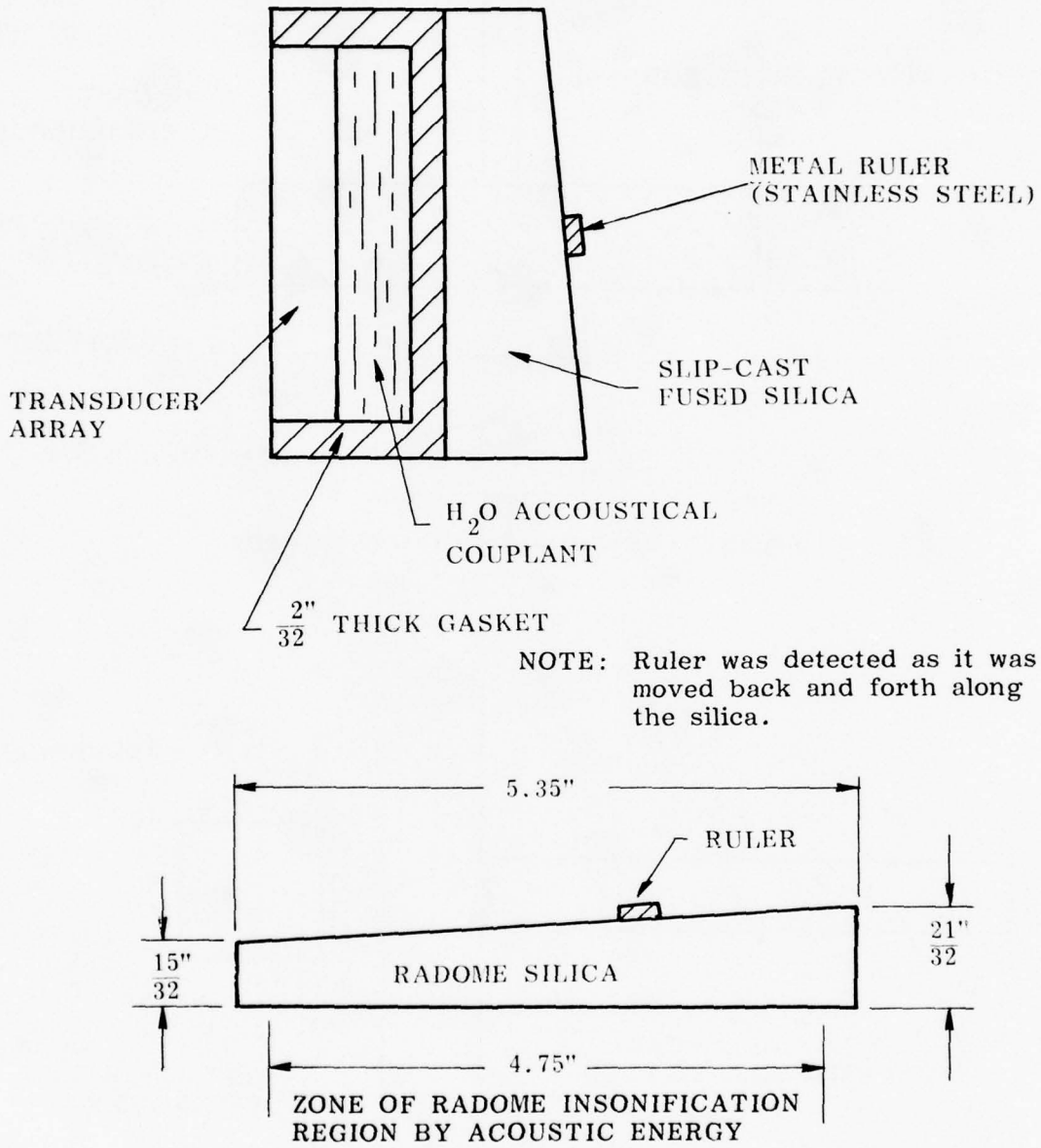

Figure 21. Acoustical Scan Test number 1 geometry.

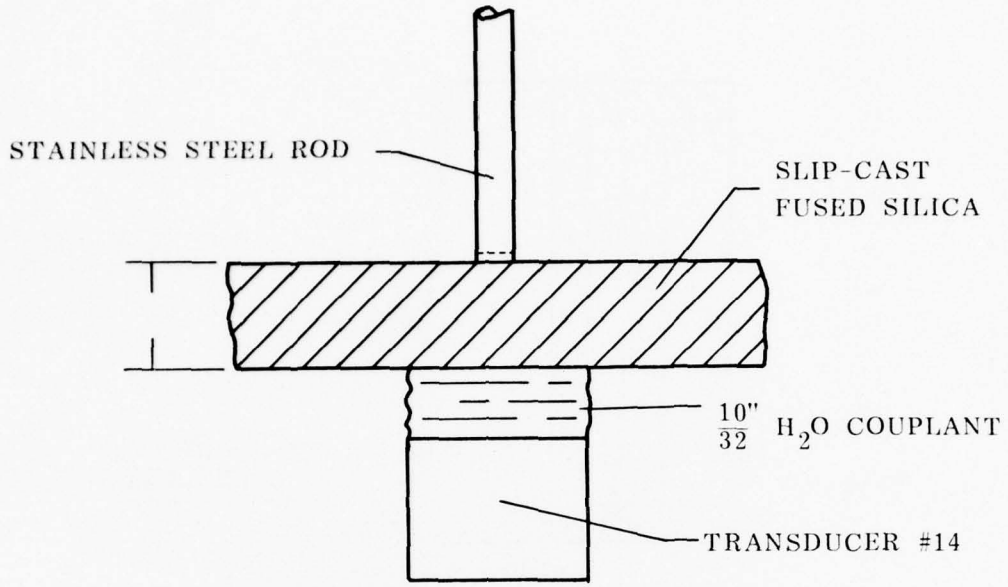

Figure 22. Acoustical Scan Test #2 geometry.

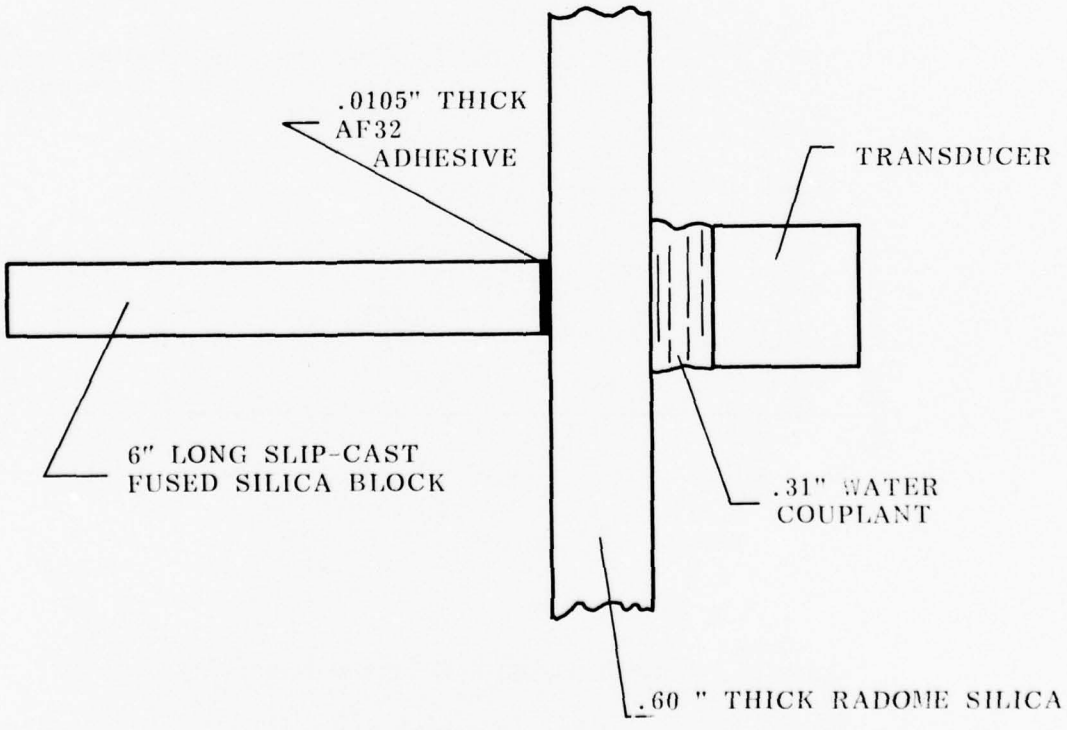

Figure 23. Acoustical Scan Test number 3 geometry.

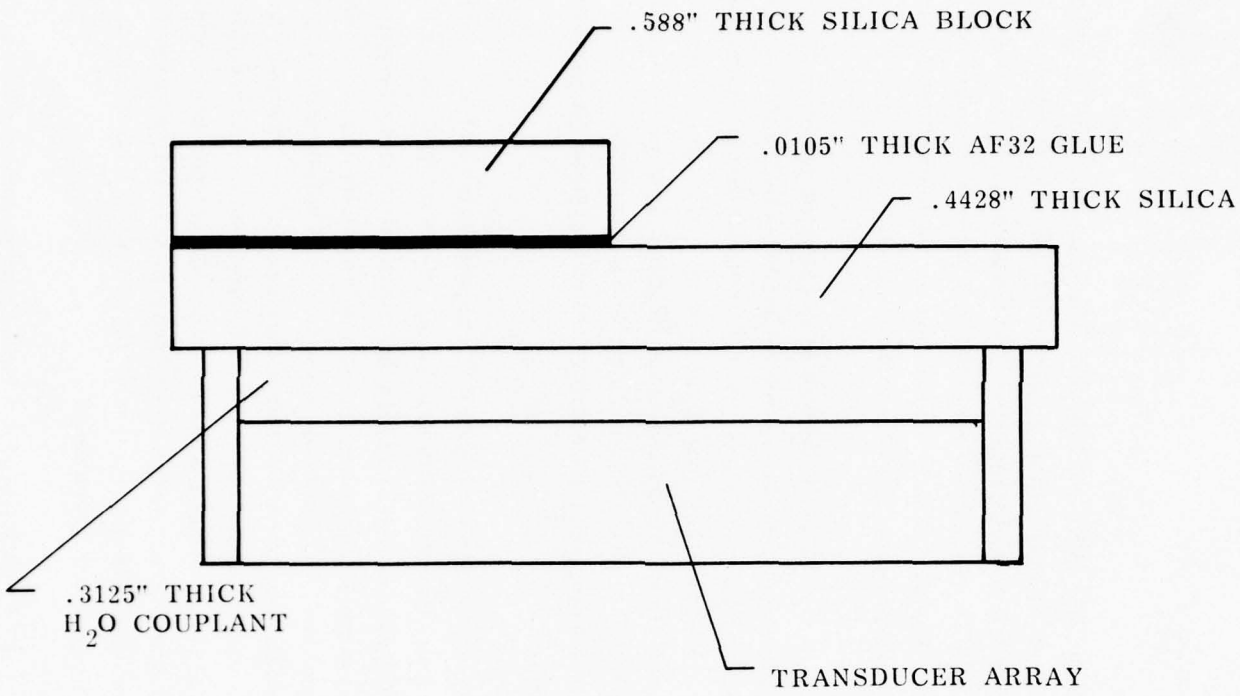

Figure 24. Acoustical Scan Test number 4 geometry.

bond. *Tables 4, 5,* and *6* show the results of these tests. As can be seen from the results in *Table 6*, $\phi\rho_\beta(1-\rho_\beta)$ gives a good description of the bond quality. From *Table 6* it is also seen that:

$$\frac{\rho_\beta|_{\text{good bond}}}{\rho_\beta|_{\text{bad bond}}} \cong \frac{.375}{.462} = .811 \quad .$$

(5) ACOUSTICAL SCAN TEST NUMBER 5. This test is the same as test number 4 except that it is in two parts. In tests with superscript-a, 0-6 transducers have the good bonds while in tests with superscript-b, 7-13 transducers have the good bonds. As can be seen from the data in *Tables 7* and *8*, the rear surface bonding can be adequately determined using the ratio of reflected echoes. Transducers 0, 1, 7 and 13 showed the poorest response due to end boundary conditions imposed on the test due to clamping, etc.

(6) ACOUSTICAL SCAN TEST NUMBER 6. In gating on a rear surface echo, the Sample and Hold circuit samples are only over several nanoseconds in duration. The effect of such a short sample period is a synthetic noise generated because the ultrasound minima and maxima do not occur at the same point in time for every scan. The variation is small but can become significant. In this test the computer gate was fixed in time and the output of the S/H circuit for transducer 0 was printed after averaging for various numbers of scans. *Table 9* tabulates the S/N ratio as a function of the number of times the output was averaged. *Figure 25* shows the results graphed.

(7) ACOUSTICAL SCAN TEST NUMBER 7. The purpose of this test was to determine the sensitivity of the array scanner system in detecting glue bond faults in the Pershing II radome glue bond line. A radome which had been sled tested and fractured was tested using the system in scope display mode. At the base of the radome, areas were mapped out where flaws were found using visual and object insertion inspection. The radome scanner system then inspected the glue bond line. A graphical picture of the glue bond line is given in *Figure 26* and a correlation of results with visual and object insertion inspection is given in *Figure 27*. In this test the amplitudes of the back surface echoes of each transducer were compared with a fixed reference level. Any time the signal amplitude exceeded the fixed level the *z*-axis scope display was turned off indicating a disbond. By varying the sensitivity level of the reference the sensitivity of the scanning system is controlled.

(8) ACOUSTIC SCAN TEST NUMBER 8. Echo patterns from selected locations on the bond line of two Pershing II radomes were mapped in an effort to determine typical readings from actual radomes. The orientation of the array relative to the radome bond line is shown in *Figure 28*.

TABLE 3. ACOUSTICAL SCAN TEST NUMBER 2 RESOLUTION

STAINLESS STEEL ROD SIZE (DIAMETER)	RESOLUTION?
14/32"	YES
11/32"	YES
9/32"	YES
7/32"	YES
5/32"	YES
3/32"	YES

NOTE: Resolution of a rod was said to exist if the back surface silica echo return decreased by 50% or more.

TABLE 4. ACOUSTICAL SCANNER TEST NUMBER 4 DATA (VALUES ARE IN VOLTS)

TRANSDUCER	I_{R1}	I_{R2}	I_{R3}	I_{R4}
0	1.9	1.30	.60	.30
1	1.8	1.15	.60	.40
2	1.8	1.40	.95	.60
3	1.7	1.10	.60	.30
4	1.75	1.20	.82	.40
5	1.75	1.20	.60	.40
6	1.95	1.50	1.10	.45
7	2.10	1.60	.80	.45
8	2.20	1.60	1.00	.45
9	2.30	1.62	.90	.45
10	2.00	1.42	.60	.45
11	2.00	1.60	1.00	.80
12	2.40	1.60	1.00	.50
13	1.95	1.40	.60	.30

TABLE 5. ACOUSTICAL SCANNER TEST NUMBER 4 DATA (VALUES ARE IN VOLTS)

TRANSDUCER	$\epsilon\rho_{B\|A}$	$\epsilon\rho_{B\|B}$	$\epsilon\rho_{B\|C}$
0	.827	.679	.707
1	.799	.722	.816
2	.882	.823	.794
3	.804	.837	.707
4	.828	.826	.698
5	.828	.707	.816
6	.877	.856	.639
7	.872	.707	.750
8	.852	.790	.670
9	.839	.745	.707
10	.842	.650	.866
11	.894	.790	.894
12	.816	.790	.707
13	.847	.654	.707

TABLE 6. ACOUSTICAL SCANNER TEST NUMBER 4 DATA (VALUES ARE IN VOLTS)

TRANSDUCER	I_{R0}	I_{R1}	$\phi\rho_B(1-\rho_B)$
0	4.95	1.90	.383
1	4.80	1.80	.375
2	4.80	1.80	.375
3	4.80	1.70	.354
4	4.80	1.75	.364
5	4.75	1.75	.368
6	4.80	1.75	.406
7	4.80	2.10	.437
8	4.90	2.20	.448
9	4.90	2.30	.469
10	4.40	2.00	.454
11	4.30	2.00	.465
12	4.80	2.40	.500
13	4.20	1.95	.464

TRANSDUCER	I_{R0}	I_{R1}	I_{R1}/I_{R0}	I_{R0}	I_{R1}	I_{R1}/I_{R0}	$\Delta(I_{R1}/I_{R0})$
0	4.85	2.50	.515	4.75	2.50	.526	.011
1	4.75	2.20	.463	4.35	2.40	.551	.088
2	4.70	2.40	.510	4.50	3.00	.666	.156
3	4.80	2.10	.437	4.40	2.95	.670	.233
4	4.65	2.30	.494	4.45	2.95	.662	.168
5	4.50	2.05	.455	4.30	2.60	.604	.149
6	4.70	2.35	.500	4.60	2.90	.630	.130
7	4.75	3.00	.631	4.60	2.75	.597	.034
8	4.80	3.10	.645	4.60	2.15	.467	.178
9	4.75	3.20	.673	4.65	2.20	.473	.200
10	4.10	2.50	.609	4.00	1.50	.375	.234
11	4.10	2.30	.560	3.90	1.50	.384	.176
12	4.60	3.00	.652	4.15	1.85	.445	.207
13	4.00	1.85	.462	4.10	1.50	.365	.097

TABLE 7. ACOUSTICAL SCAN TEST NUMBER 5 DATA (ALL VALUES IN VOLTS)

TABLE 8. ACOUSTICAL SCAN TEST NUMBER 5 DATA

TRANSDUCER	$\frac{\rho_B \mid GOOD}{\rho_B \mid BAD}$	TRANSDUCER	$\frac{\rho_B \mid GOOD}{\rho_B \mid BAD}$
0	.979	7	.946
1	.840	8	.724
2	.765	9	.702
3	.652	10	.615
4	.746	11	.685
5	.753	12	.682
6	.793	13	.790

TABLE 9. S/N RATIO AS A FUNCTION OF NUMBER OF SCAN AVERAGES

NUMBER OF SCAN AVERAGES	MAXIMUM SIGNAL DEVIATION*	AVERAGE OF SIGNAL @ MAXIMUM AND MINIMUM CONDITIONS*	SIGNAL/NOISE (S/N RATIO)
1	199	685.5	3.447
3	116	677	5.836
10	73	644.5	8.828

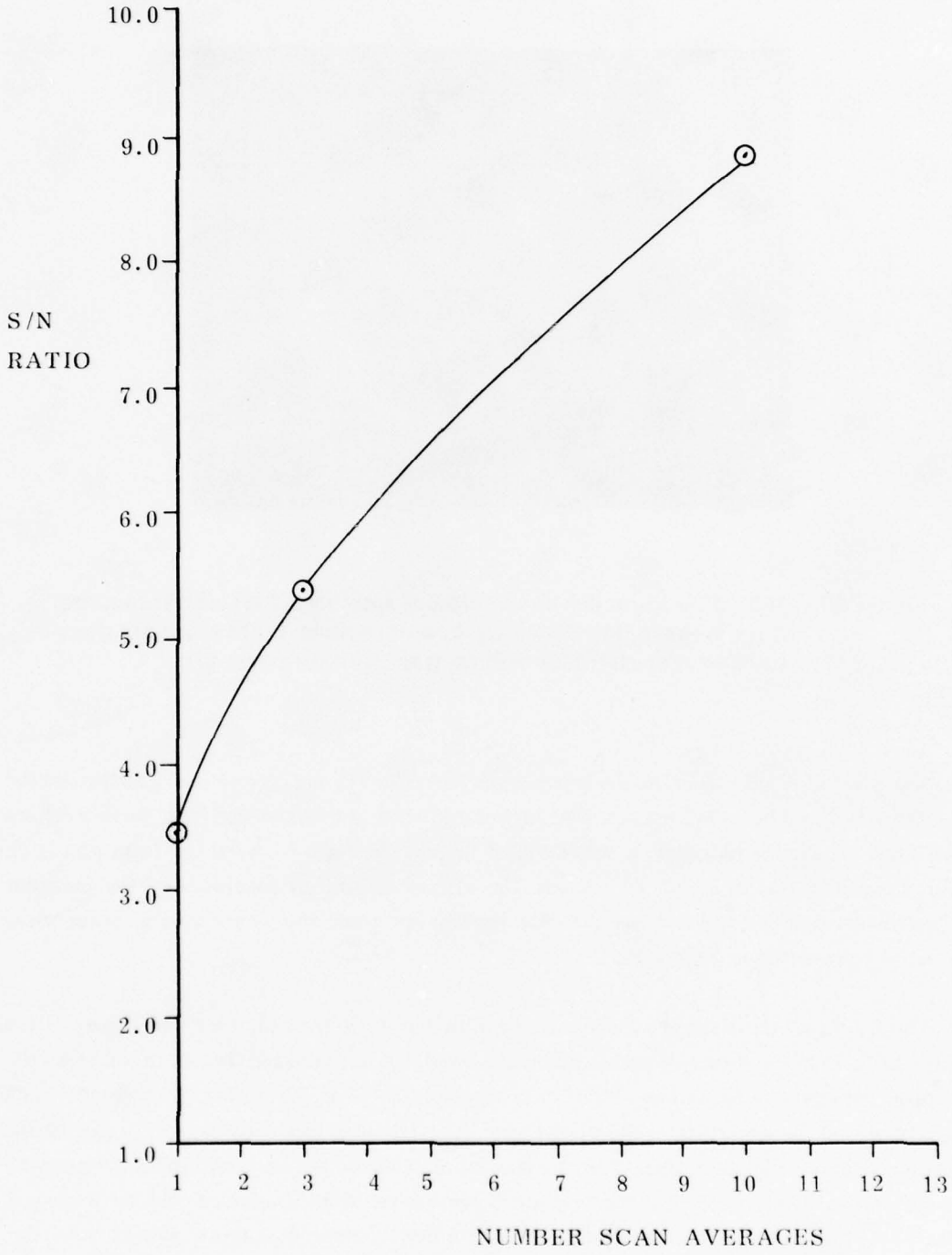

Figure 25. S/N ratio versus number of scan averages of transducer 0.

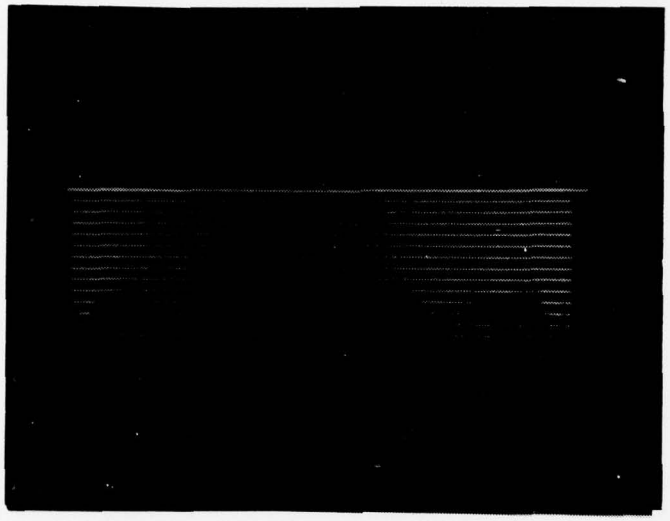

Figure 26. 360° glue bond line inspection of fractured Pershing II radome. Dark areas in line traces are flawed regions. Light areas are good bonded material. The bottom trace is transducer 0.

The procedure was to manually select transducers on the array, and then to measure the front surface and bond line echoes. Due to the large observed variation in front surface echoes for these particular radomes, it was decided to plot the ratio between the front and back surface echoes in an effort to remove the effects of non-uniformities in the transmit transducers and the radome surface. An oscilloscope trace showing a typical sequence of echoes is presented in *Figure 29*.

The results of these studies are summarized in *Figure 30* for radome 1 and *Figure 31* for radome 2. In both cases only points below the bond line were plotted. For both radomes, the typical pattern was to obtain a ratio of ρ between. .3 - .4 at the botton of the joint which gradually fell to about .03 - .05 at the top. It is felt that this drop is simply due to the geometrical misalignment caused by the curvature in the bond line, demonstrated by the ray trace shown in *Figure 8*. Experiments were performed which indicated that by angling a transducer at about 6° to the silica at the upper bond positions, a much greater bond line reflection could be obtained. It is essential that the bond line reflection be reasonably strong and uniform in order to pick out anomalies due to flaw conditions.

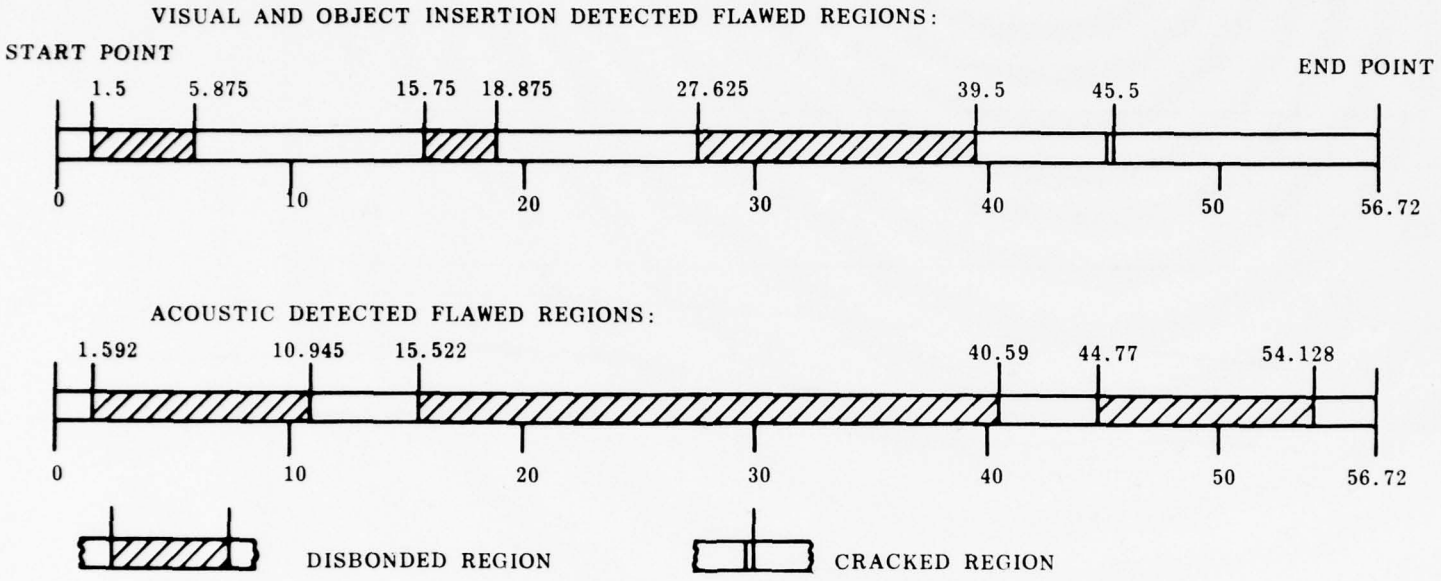

Figure 27. 360° comparison of bond faults in Pershing II radome using acoustic and manual inspection. All dimensions are in inches. Note that the acoustic method located more disbonds.

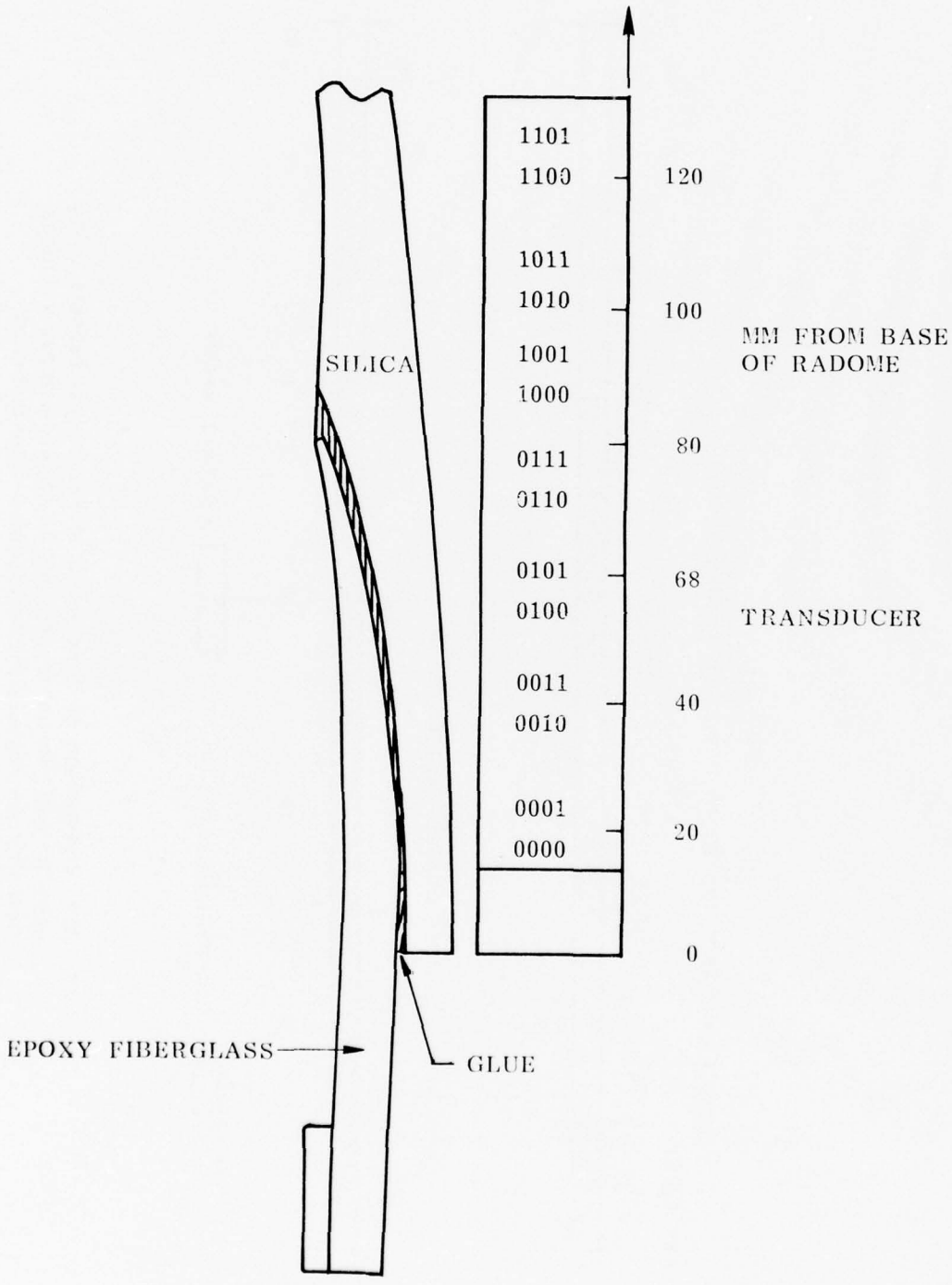

Figure 28. Orientation of array at the base of the radome.

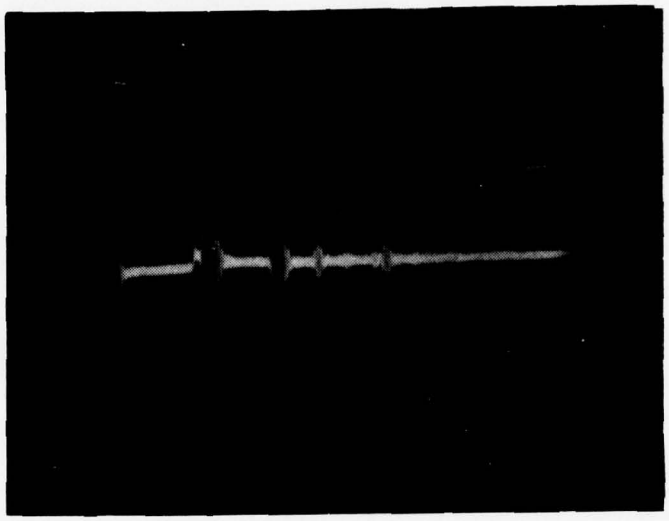

Figure 29. Typical sequence of echoes obtained with transducer 0111 at 2.00 inches on the glue bond line of radome 1. The first burst on the left is the transducer transmit pulse. The succeeding pulses are:

- **glitch from gate**
- **water-silica echo**
- **bond line echo**
- **first reverberation of water silica echo**
- **reverberation of bond line echo**
- **second reverberation of water-silica echo.**

(9) ACOUSTICAL SCAN TEST NUMBER 9. In this test four transducer scans were made of glue-fiberglass interface. The scans were made 6.5 μs after the receipt of the front surface echo. As can be seen in *Figures 32* and *33* the scanning technique was to plot the Sample and Hold output versus scan angle θ of the radome. Regions of high amplitude are desired for this indicates good glue bonding at the silica-glue interface. To make these plots the scanner was turned on and the Sample and Hold gate was set on the glue-fiberglass echo peak. As the radome rotated the Sample and Hold output was plotted on a digital oscilloscope.

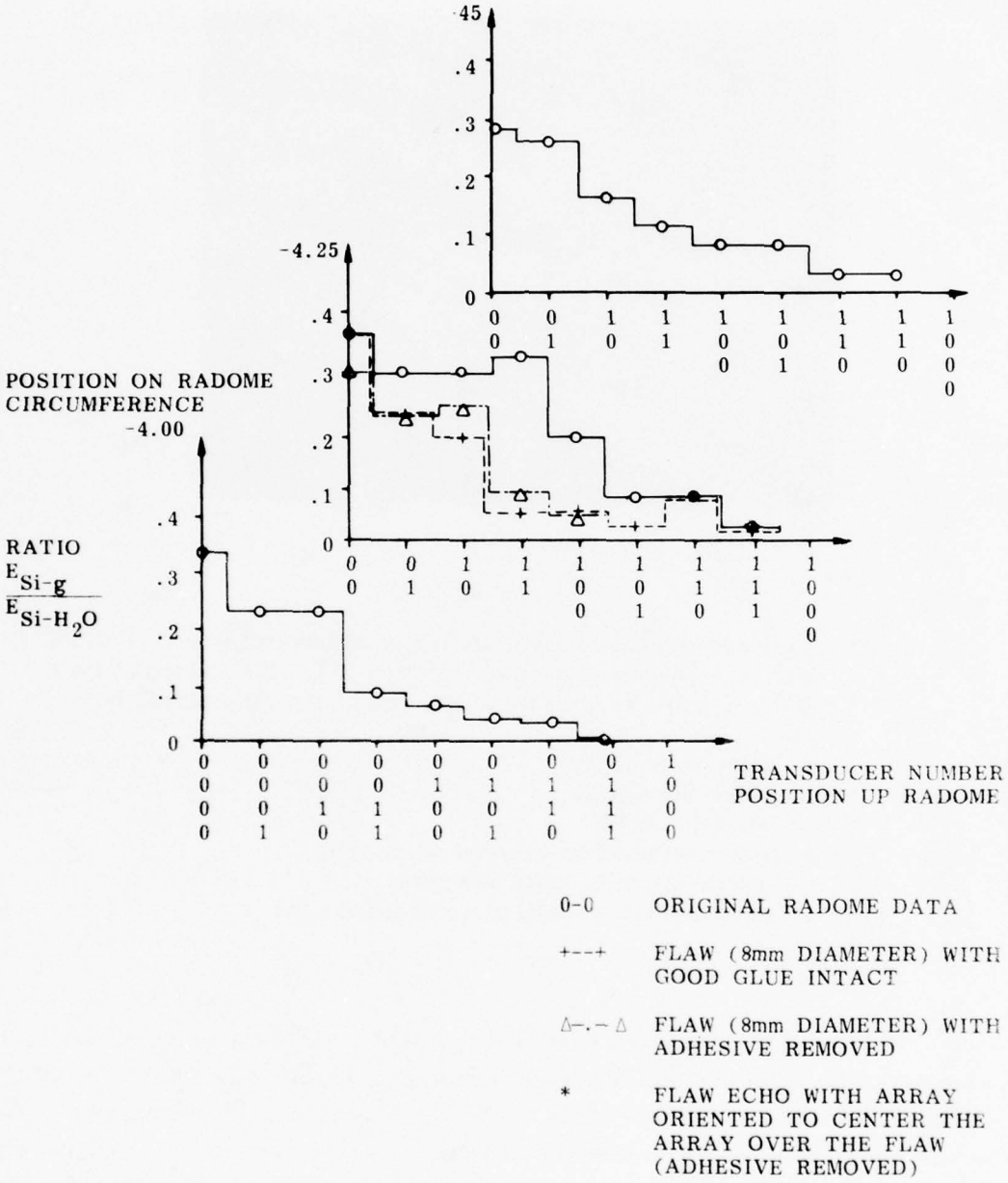

Figure 30. Mapping of front surface to bond line echo ratios for three positions on radome number 1. At the -4.25 inch position, a flaw was produced by boring through the fiberglass with a moto-tool. Initially the flaw produced a drop in return, but with proper orientation of the array, it resulted in an increased echo.

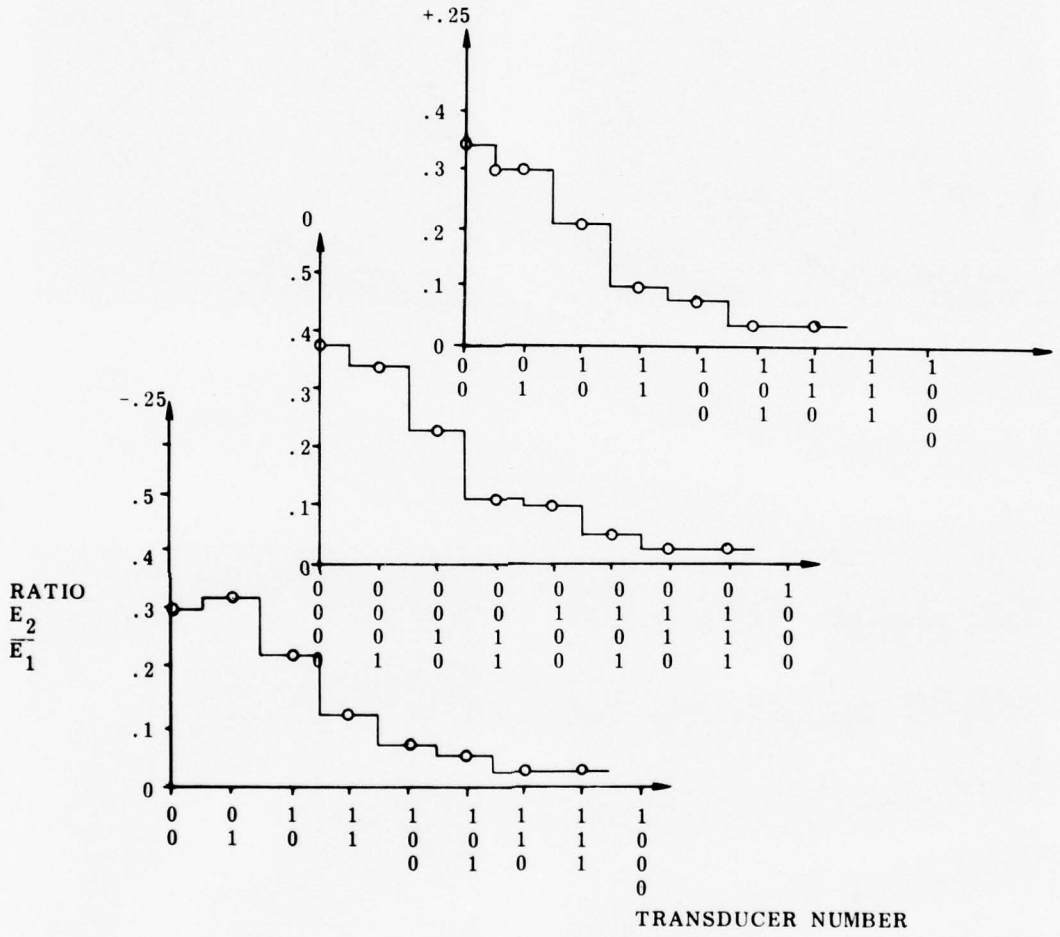

Figure 31. Mapping of front surface to bond line echo ratios for three positions on radome number 2. Note the general downward trend in the echo ratios is quite similar to that noted on radome number 1, suggesting that this is a general characterisitic of Pershing II radomes.

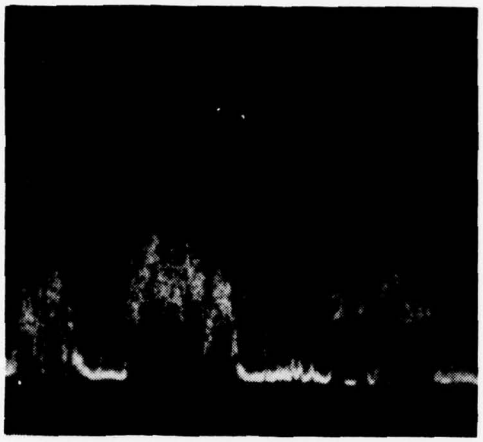

Transducer O

Transducer 1

Transducer 2

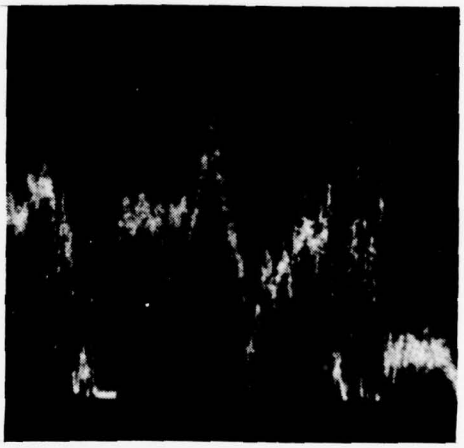

Transducer 3

Figure 32. Acoustical echo level from fiberglass-glue bond line. A high echo return in this case is characteristic of a good bond at the silica-glue interface. The Sample and Hold was made 6.5 μs after receipt of the front surface echo.

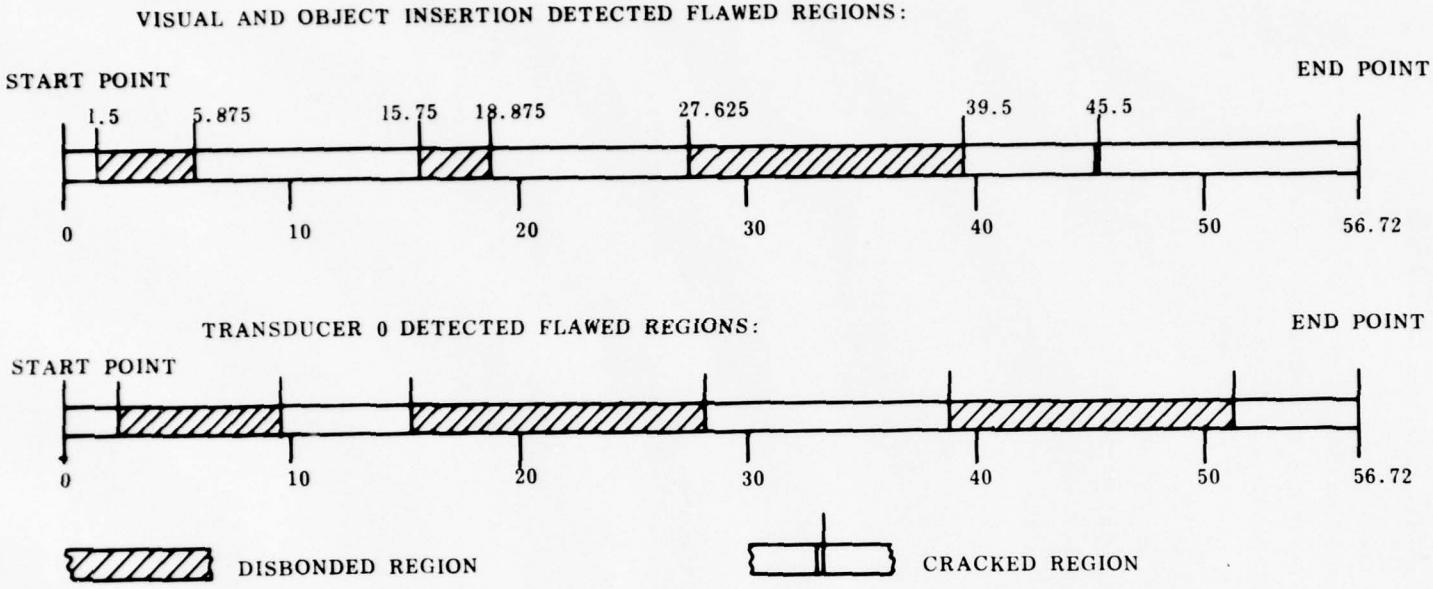

Figure 33. Flawed regions detected by transducer 0 located .725 inch from the base of the silica. All scanning was at the fiberglass-glue interface. The acoustic scan is considered to be the most reliable flaw detection method.

5. SUMMARY AND CONCLUSIONS

An attempt to bring together the pertinent theory, a description of the ultrasonic radome inspection system and the results of various tests to evaluate the system has been made. A major question, partially answered by the studies performed, concerns the nature of the bond region. For radome 1, neutron radiographs were available and they revealed a highly nonhomogenous structure in the bond line region. Large bubbles, several millimeters to several centimeters in diameter appeared to be typical and areas of solid glue were the exception. Since radiographs give no depth information, it could not be determined whether these bubbles were located in the glue or at either of the two interfaces. The theory predicts a front surface-back surface echo ratio of .4 for a good glue joint and values of .3 - .4 were typical for the regions near the bottom of the radome where the pulse was reasonably normal to the bond line.

Transmission studies, on the other hand generally gave very poor transmission coefficients (.1 or less) except for a few selected areas. It may be then that the inclusions in the glue are generally not located at the glue-silica interface, but deeper in the glue layer. Phase reversals were quite common in the glue joint echo, suggesting that such inclusions were present somewhere in the glue joint. It would be useful to microtone sections of the bond line, examine them microscopically and correlate the results with the received echoes. In general, however, the regularity of the results at the bottom of the bond line suggests a reasonably uniform return could be obtained with appropriate alignment of the beam directions using an acoustic lens.

Given the available data, a number of conclusions can be derived from this study. First, it is possible to detect and differentiate a number of different types of flaws in radome bond lines. Second, computer processing can significantly enhance the results of scanning. With the computer controlled gate a scan can be made throughout the bond line region revealing the anomalies and their dimensions. Finally, without any modifications, the present system can perform an excellent job of detecting flaws and inclusions. Preliminary work not reported here shows that the system can also scan composites with very good accuracy.

6. FUTURE AREAS OF RESEARCH

Additional work on the system should focus on the areas of improved transducer uniformity, particularly in damping, higher frequency arrays for better depth resolution, the use of computer processing of the RF echo bursts to enhance detection and differentiation of flaws and the investigation of better display modes. Even without these improvements the present system has a great deal of detection capability. Several improvements could also be

made in the scanning electronics. Individual preamps and balance networks for the transducers would be desired. Also smaller transducers and a larger number of transducers would further enhance resolution. Finally it would be useful to production engineer the system to increase its overall reliability and get it into field use. The production engineering procedure should include the integration of a microprocessor into the system to cut the cost of using a larger computer.

REFERENCES

1. Brekhovskikh, Leonid M., *Waves In Layard Media*, Academic Press, 1960.

2. Fox, M. D., "Design for a 25 Element Linear Array for Scanning Bond Lines in Ceramic Radomes," *Micom Internal Technical Report*, 31 July 1975.

3. Himes, D., *Signal Processor and Array Non-Destructive Test System Technical Manual*, July 1978, Technical Report No. SP-220-1026.

APPENDIX

The computer codes on the following pages were developed to perform specialized scanning operations using a PDP11-40 controller. Five programs were developed and are presented as Fortran IV code. *Figure 34* shows the basic system layout for using a PDP11-40 controller for scan control. A DRII-C and ARII lab interface package manufactured by Digital Equipment Corporation was used for analog and digital interfacing to a PDP11-40 controller.

Program: ARRAY. FOR

Purpose: Sample and Hold Scanning of a point in the return echo. The gate is set at the scan controller.

Input:

(1) Number of transducers—Up to 14 transducers may be scanned always starting with transducer 0 located at the radome base.

(2) Voltage Trigger Level—the digital value of the scan controller clock voltage; anywhere between 700 and 1023.

(3) Number steps/scan—Number of discrete advances of the radome between scans. 31000 advances equals one revolution (2π) of the radome.

(4) Step rate—rate at which the radome is moved between scans. Values are from 10 to 200.

(5) Number Scan Points—total number of points to be scanned.

(6) Print data—request for data to be printed on the teleprinter.

Output: (1) data is printed on a decwriter.
(2) data is plotted on a scope.

```
TT:=DX1:ARRAY.FOR
      DIMENSION ID(14),ID1(14,500)
      WRITE(5,1)
1     FORMAT(' RADOME SCANNER ARRAY SIGNAL PROCESSOR')
      WRITE(5,2)
2     FORMAT(' INPUT THE FOLLOWING DATA:')
      WRITE(5,3)
```

*OPTIONAL EQUIPMENT

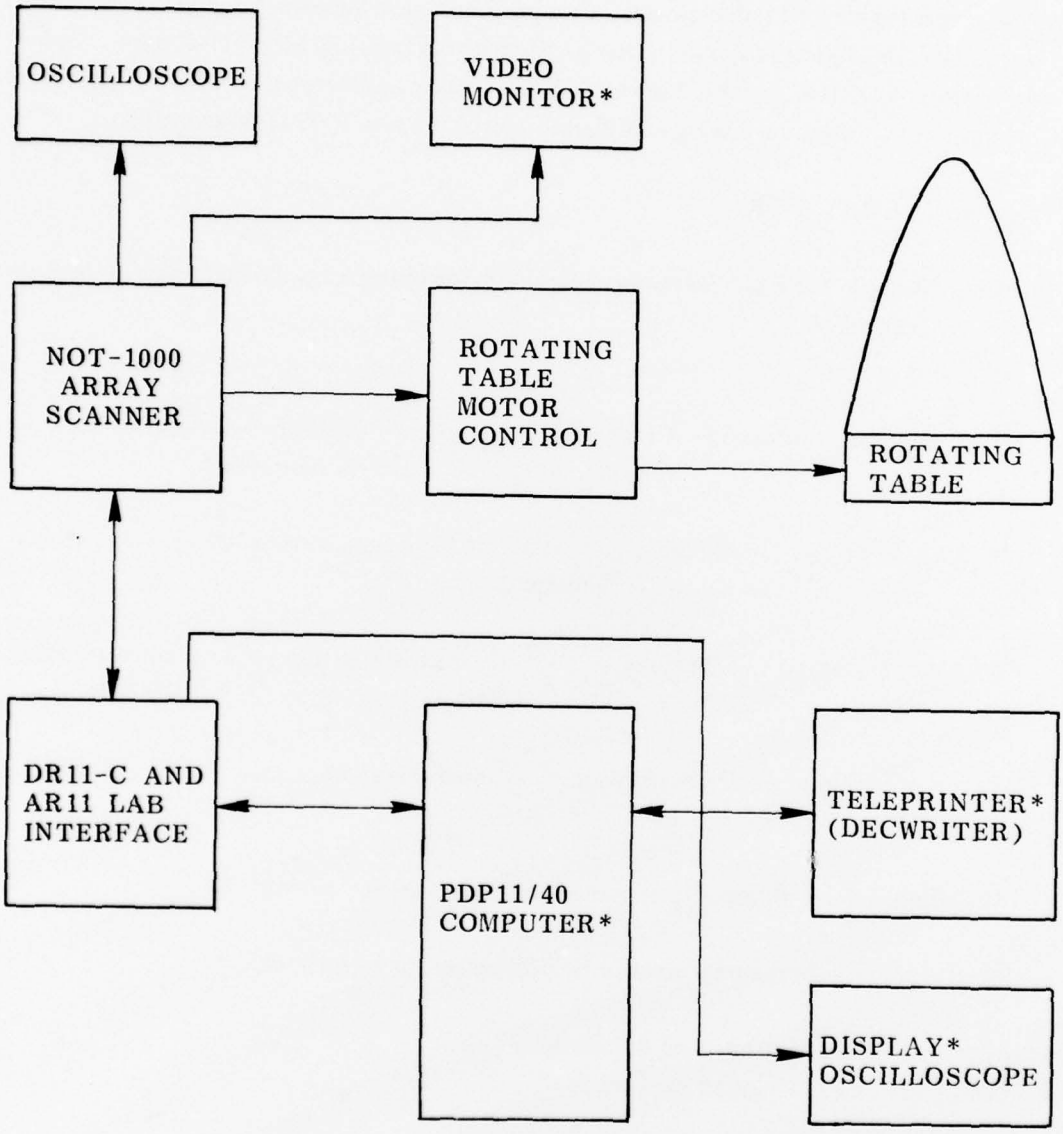

Figure 34. System for computer data processing.

```
3       FORMAT(' NUMBER OF TRANSDUCERS?-I3')
        READ(5,4) NT
4       FORMAT(I3)
        WRITE(5,5)
5       FORMAT(' VOLTAGE TRIGGER LEVEL-I3')
        READ(5,4) NL
         WRITE(5,11)
11       FORMAT(25H INPUT NO. STEPS/SCAN:-I3)
         READ(5,12) IS
12       FORMAT(I3)
         WRITE(5,13)
13       FORMAT(20H INPUT STEP RATE:-I3)
         READ(5,12) ISR
        WRITE(5,18)
18      FORMAT(23H INPUT NO. SCAN PTS.-I3)
        READ(5,4) NP
        WRITE(5,19)
19      FORMAT(18H PRINT DATA? 1=YES)
        READ(5,20) IPC
20      FORMAT(I1)
        NC=1
6        CALL IPOKE("167772,"000002)
        CALL IPOKE("167772,"000000)
16        CALL IPOKE("170400,"21001)
         IT=IPEEK("170402)
         IF(IT.LT.NL) GOTO 16
         DO 9 I=1,NT,1
7        CALL IPOKE("170400,"21001)
         IT=IPEEK("170402)
         IF(IT.GT.NL) GOTO 7
         ID(I)=IT
8         CALL IPOKE("170400,"21001)
         IT=IPEEK("170402)
         IF(IT.GT.NL) GOTO 9
         IF(ID(I).GT.IT) ID(I)=IT
        ID1(I,NC)=ID(I)
         IF(I.EQ.NT) GOTO 9
         GOTO 8
9        CONTINUE
        IF(IPC.NE.1) GOTO 21
         WRITE(5,10) NC,(ID(JJ),JJ=1,NT,1)
10       FORMAT(1H ,21I5)
21       CONTINUE
        NC=NC+1
        IF(NC.GT.NP) GOTO 24
        DO 14 ISS=1,IS,1
         CALL IPOKE("167772,"000001)
         DO 15 ID3=1,ISR,1
15       Y=SIN(3.14159)
```

```
        CALL IPOKE("167772,"000000)
        DO 17 ID2=1,ISR,1
17      Y=SIN(3.14159)
14      CONTINUE
        GOTO 6
24      CONTINUE
       WRITE(5,22)
22     FORMAT(28H TRANSDUCER FOR PLOTTING-I2:)
       READ(5,23) ITP
23     FORMAT(I2)
       IF(ITP.LE.0.OR.ITP.GE.15) GOTO 27
26      CONTINUE
        CALL IPOKE("170412,"500)
       DO 25 J=1,NF,1
       IMT=ID1(ITP,J)
       CALL IPOKE("170412,IMT)
25     CONTINUE
       CALL IPOKE("170412,"0)
       ITEST=IPEEK("177570)
       IF(ITEST.EQ.1) GOTO 24
       GOTO 26
27      CONTINUE
        END
*
```

Program: LOCAT. FOR

Purpose: Positions the computer gate for the Sample and Hold. The gate is positioned by typing in a value of 1 to 1024. This is used to locate the gate positions of the front and back ceramic radome echoes for ratio scanning.

Input: Gate Position—a value of 1 to 1023.

Output: Gate is positioned.

```
 TT:=DX1:LOCAT.FOR
C------GATE POSITIONING PROGRAM FOR ARRAY SCANNER
1      READ(5,2) N
2      FORMAT(I5)
       CALL IPOKE("170412,N)
       GOTO 1
       END
*
```

Program: ARRAY1. FOR

Purpose: This program compares the ratio of a back surface echo amplitude to the front surface echo amplitude. Scanning is done in Sample and Hold mode.

Input:

(1) Number of Transducers—up to 14 transducers may be scanned starting with transducer 0 located at the radome base.

(2) Trigger Level—the digital valve of the scan controller clock voltage; anywhere between 700 and 1023.

(3) Number Scan Points—total number of points to be scanned.

(4) Number Steps/Scan—number of discrete advances of the radome between scans. 31000 advances equals one revolution (2π) of the radome.

(5) Step Delay—rate at which the radome is moved between scans. Values are from 10 to 200.

(6) Gate Position-1—Sample and Hold gate location (0-1023) of the echo for the denominator term in echo ratio testing.

(7) Gate Position-2—Sample and Hold gate location (0-1023) of the echo for the numerator term in echo ratio testing.

(8) Gate Settle Delay—delay allowed for the computer controlled gate to settle (normally 10).

Output:

(1) If any bit of the PDP11-40 control console is high, data is printed on a decwriter.

(2) Data is plotted on a scope for each transducer.

```
TT:=DX1:ARRAY1.FOR
      DIMENSION IBB(14),IB(14),IC(14,500)
      WRITE(5,1)
1     FORMAT(' RADOME ARRAY SCANNER SYSTEM')
      WRITE(5,2)
```

```
2     FORMAT(' INPUT NO. OF TRANSDUCERS?')
      READ(5,3) N1
3     FORMAT(I5)
      WRITE(5,4)
4     FORMAT(' TRIGGER LEVEL?')
      READ(5,3) N3
      WRITE(5,5)
5     FORMAT(' NO. SCAN POINTS?')
      READ(5,3) N5
      WRITE(5,6)
6     FORMAT(' NO. STEPS/SCAN?')
      READ(5,3) N4
      WRITE(5,7)
7     FORMAT(' STEP DELAY?')
      READ(5,3) N6
      WRITE(5,8)
8     FORMAT(' GATE POSITION-1?')
      READ(5,3) N7
      WRITE(5,9)
9     FORMAT(' GATE POSITION-2?')
      READ(5,3) N8
      WRITE(5,20)
20    FORMAT(' GATE SETTLE DELAY?')
      READ(5,3) N11
      DO 11 I=1,N5,1
      CALL ASCAN(N1,N3,IBB,N7,N11)
      CALL ASCAN(N1,N3,IB,N8,N11)
      DO 10 J=1,N1,1
      IF(IBB(J).EQ.0) IBB(J)=1
      A=FLOAT(IB(J))/FLOAT(IBB(J))
      IF(ABS(A).GT.1.024) A=1.024
      IC(J,I)=INT(1000.*A)
      ITEST=IPEEK("177570)
      IF(ITEST.EQ.0) GOTO 10
      WRITE(5,19) IBB(J),IB(J),IC(J,I)
19    FORMAT(3I5)
10    CONTINUE
      CALL AMOVE(N4,N6)
11    CONTINUE
12    WRITE(5,13)
13    FORMAT(' TRANSDUCER FOR PLOTTING?')
      READ(5,3) ITP
      IF(ITP.LE.0.OR.ITP.GE.N1) GOTO 16
14    CONTINUE
      CALL IPOKE("170414,"777)
      DO 15 I=1,N5,1
      IMT=IC(ITP,I)
15    CALL IPOKE("170414,IMT)
      CALL IPOKE("170414,"0)
```

```
      ITEST=IPEEK("177570)
      IF(ITEST.EQ.0) GOTO 14
      GOTO 12
16    CONTINUE
      DO 18 I=1,N5,1
      WRITE(5,17) I, (IC(J,I), J=1,N1,1)
17    FORMAT(I5,14I5)
18    CONTINUE
      STOP
      END
      SUBROUTINE ASCAN(N1,N3,N9,N10,N11)
      DIMENSION N9(14)
      CALL IPOKE("170412,N10)
      DO 5 I=1,N11,1
      DO 5 J=1,N11,1
      DO 5 K=1,N11,1
5     CONTINUE
      CALL IPOKE("167772,"2)
      CALL IPOKE("167772,"0)
1     CALL IPOKE("170400,"21001)
      IT=IPEEK("170402)
      IF(IT.LT.N3) GOTO 1
      DO 4 I=1,N1,1
2     CALL IPOKE("170400,"21001)
      IT=IPEEK("170402)
      IF(IT.GT.N3) GOTO 2
      N9(I)=IT
3     CALL IPOKE("170400,"21001)
      IT=IPEEK("170402)
      IF(IT.GT.N3) GOTO 4
      IF(N9(I).GT.IT) N9(I)=IT
      IF(I.EQ.N1) GOTO 4
      GOTO 3
4     CONTINUE
      RETURN
      END
      SUBROUTINE AMOVE(N4,N6)
      DO 3 I=1,N4,1
      CALL IPOKE("167772,"1)
      DO 1 J=1,N6,1
1     CONTINUE
      CALL IPOKE("167772,"0)
      DO 2 J=1,N6,1
2     CONTINUE
3     CONTINUE
      RETURN
      END
*
```

Program: ARRAY2. FOR

Purpose: This program compares the ratio of a back surface echo amplitude to the front surface echo amplitude. Scanning is done in Sample and Hold mode. Multiple Sample and Hold averages can be made at a single gate location.

Input:

(1) Number of Transducers—up to 14 transducers may be scanned starting with transducer 0 located at the radome base.

(2) Trigger Level—the digital value of the scan controller clock voltage; anywhere between 700 and 1023.

(3) Number Scan Points—total number of points to be scanned.

(4) Number Steps/Scan—number of discrete advances of the radome between scans. 31000 advances equals one revolution (2π) of the radome.

(5) Step Delay—rate at which the radome is moved between scans. Values are from 10 to 200.

(6) Gate Position-1—Sample and Hold gate location (0-1023) of the echo for the denominator term in echo ratio testing.

(7) Gate Position-2—Sample and Hold gate location (0-1023) of the echo for the numerator term in echo ratio testing.

(8) Gate Settle Delay—delay allowed for the computer controlled gate to settle (normally 10).

(9) Samples/Scan Point—to increase the Signal/Noise ratio, each gate position is scanned a multiple number of times and an average value of the echo return is computed. The number of samples composing the average is given as input here.

Output:

(1) If any bit on the PDP11-40 control console is high, data is printed on a decwriter.

(2) Data is plotted on a scope for each transducer.

```
 TT:=DX1:ARRAY2.FOR
      DIMENSION IBB(14),IB(14),IC(14,500)
22    WRITE(5,1)
1     FORMAT(' RADOME ARRAY SCANNER SYSTEM')
      WRITE(5,2)
2     FORMAT(' INPUT NO. OF TRANSDUCERS?')
      READ(5,3) N1
3     FORMAT(I5)
      WRITE(5,4)
4     FORMAT(' TRIGGER LEVEL?')
      READ(5,3) N3
      WRITE(5,5)
5     FORMAT(' NO. SCAN POINTS?')
      READ(5,3) N5
      WRITE(5,6)
6     FORMAT(' NO. STEPS/SCAN?')
      READ(5,3) N4
      WRITE(5,7)
7     FORMAT(' STEP DELAY?')
      READ(5,3) N6
      WRITE(5,8)
8     FORMAT(' GATE POSITION-1?')
      READ(5,3) N7
      WRITE(5,9)
9     FORMAT(' GATE POSITION-2?')
      READ(5,3) N8
      WRITE(5,20)
20    FORMAT(' GATE SETTLE DELAY?')
      READ(5,3) N11
      WRITE(5,21)
21    FORMAT(' NO. OF SAMPLES/SCAN PT.?')
      READ(5,3) N12
      DO 11 I=1,N5,1
      CALL ASCAN(N1,N3,IBB,N7,N11,N12)
      CALL ASCAN(N1,N3,IB,N8,N11,N12)
      DO 10 J=1,N1,1
      IF(IBB(J).EQ.0) IBB(J)=1
      A=FLOAT(IB(J))/FLOAT(IBB(J))
      IF(ABS(A).GT.1.024) A=1.024
      IC(J,I)=INT(1000.*A)
      ITEST=IPEEK("177570)
      IF(ITEST.EQ.1) GOTO 22
      IF(ITEST.EQ.0) GOTO 10
      WRITE(5,19) I,IBB(J),IB(J),IC(J,I)
19    FORMAT(4I5)
10    CONTINUE
      CALL AMOVE(N4,N6)
11    CONTINUE
12    WRITE(5,13)
```

```
13      FORMAT(' TRANSDUCER FOR PLOTTING?')
        READ(5,3) ITP
        IF(ITP.LE.0.OR.ITP.GT.N1) GOTO 16
14      CONTINUE
        CALL IPOKE("170414,"777)
        DO 15 I=1,N5,1
        IMT=IC(ITP,I)
15      CALL IPOKE("170414,IMT)
        CALL IPOKE("170414,"0)
        ITEST=IPEEK("177570)
        IF(ITEST.EQ.0) GOTO 14
        GOTO 12
16      CONTINUE
        DO 18 I=1,N5,1
        WRITE(5,17) I,-(IC(J,I),-J=1,N1,1)------
17      FORMAT(I5,14I5)
18      CONTINUE
        STOP
        END
        SUBROUTINE ASCAN(N1,N3,N9,N10,N11,N12)
        DIMENSION N9(14),N13(14)
        DO 6 I=1,N1,1
6       N9(I)=0
        DO 7 L=1,N12,1
        CALL IPOKE("170412,N10)
        DO 5 I=1,N11,1
        DO 5 J=1,N11,1
        DO 5 K=1,N11,1
5       CONTINUE
        CALL IPOKE("167772,"2)
        CALL IPOKE("167772,"0)
1       CALL IPOKE("170400,"21001)
        IT=IPEEK("170402)
        IF(IT.LT.N3) GOTO 1
        DO 4 I=1,N1,1
2       CALL IPOKE("170400,"21001)
        IT=IPEEK("170402)
        IF(IT.GT.N3) GOTO 2
        N13(I)=IT
3       CALL IPOKE("170400,"21001)
        IT=IPEEK("170402)
        IF(IT.GT.N3) GOTO 4
        IF(N13(I).GT.IT) N13(I)=IT
        IF(I.EQ.N1) GOTO 4
        GOTO 3
4       CONTINUE
        DO 7 LL=1,N1,1
7       N9(LL)=N9(LL)+N13(LL)
        DO 8 I=1,N1,1
```

```
3       N9(I)=N9(I)/N1
        RETURN
        END
        SUBROUTINE AMOVE(N4,N6)
        DO 3 I=1,N4,1
        CALL IPOKE("167772,"1)
        DO 1 J=1,N6,1
1       CONTINUE
        CALL IPOKE("167772,"0)
        DO 2 J=1,N6,1
2       CONTINUE
3       CONTINUE
        RETURN
        END
*
```

Program: ARRAY3. FOR

Purpose: This program rotates the radome and transmits scan pulses to control scanning. All signal processing of the echo returns is done external to the computer.

Input:

(1) Number Scan Points—total number of points to be scanned.

(2) Number Motor Pulses/Scan—number of discrete advances of the radome between scans. 31000 advances equals one revolution (2π) of the radome.

(3) Motor Pulse Width—duration of motor pulses (10-200).

```
 TT:=ARRAY3.FOR
C-----ARRAY3 SCANNER ARRAY CODE
C-----WRITTEN BY: JOHN A. SCHAEFFEL, JR.
      WRITE(5,1)
1     FORMAT(' INPUT NO. SCAN POINTS:')
      READ(5,2) N
2     FORMAT(I4)
      WRITE(5,3)
3     FORMAT(' INPUT NO. MOTOR PULSES/ SCAN:')
      READ(5,2) M
      WRITE(5,4)
4     FORMAT(' INPUT MOTOR PULSE WIDTH:')
      READ(5,2) L
```

```
8       CONTINUE
        DO 7 I=1,N,1
        CALL IPOKE("170412,I)
        CALL IPOKE("167772,"2)
        CALL IPOKE("167772,"0)
        DO 7 J=1,M,1
        CALL IPOKE("167772,"1)
        DO 5 K=1,L,1
5       CONTINUE
        CALL IPOKE("167772,"0)
        DO 6 K=1,L,1
6       CONTINUE
7       CONTINUE
        ITEST=IPEEK("177570)
        IF(ITEST.NE.0) GOTO 8
        STOP
        END
*
```

DISTRIBUTION

	No. of Copies
Defense Metals Information Center Battelle Memorial Institute 505 King Avenue Columbus, Ohio 43201	1
Defense Documentation Center Cameron Station Alexandria, Virginia 22314	12
Commander Us Army Foreign Science and Technology Center ATTN: DRXST-SD3 220 Seventh Street, NE Charlottesville, Virginia 22901	1
Office of Chief of Research and Development Department of the Army ATTN: DARD-ARS-P Washington, D. C. 20301	1
Commander US Army Electronics Command ATTN: DRSEL-PA-P DRSEL-CT-DT DRSEL-PP, Mr. Sulkolove Fort Monmouth, New Jersey 07703	1 1 1
Commander US Army Natick Laboratories Kansas Street ATTN: STSNLT-EQR Natick, Massachusetts 01760	1
Commander US Army Mobility Equipment Research and Development Center Fort Belvoir, Virginia 22060	1
Director USA Mobility Equipment Research and Development Center Coating and Chemical Laboratory ATTN: STSFB-CL Aberdeen Proving Ground, Maryland 21005	1
Commander Edgewood Arsenal ATTN: SAREA-TS-A Aberdeen Proving Ground, Maryland 21010	1
Commander Picatinny Arsenal ATTN: SARPA-TS-S, Mr. M. Costello Dover, New Jersey 07801	1
Commander Rock Island Arsenal Research and Development ATTN: 9320 Rock Island, Illinois 61201	1
Commander Watervliet Arsenal Watervliet, New York 12189	1
Commander US Army Aviation Systems Command ATTN: DRSAV-EE DRSAV-ER, Mr. Vollmer St. Louis, Missouri 63166	1 1
Commander US Army Aeronautical Depot Maintenance Center (Mail Stop) Corpus Christi, Texas 78403	1
Commander US Army Test and Evaluation Command ATTN: DRSTE-RA Aberdeen Proving Ground, Maryland 21005	1
Commander US Army White Sands Missile Range ATTN: STEWS-AD-L White Sands Missile Range, New Mexico 88002	1
Commander ATTN: STEAP-MT Aberdeen Proving Ground, Maryland 21005	1
Chief Bureau of Naval Weapons Department of the Army Washington, D. C. 20390	1
Chief Bureau of Ships Department of the Navy Washington, D. C. 20315	1

DISTRIBUTION (Continued)

	No. of Copies
Naval Research Laboratory ATTN: Dr. M. M. Krafft Code 8430 Washington, D. C. 20375	1
Commander Wright Air Development Division ATTN: ASRC Wright-Patterson AFB, Ohio 45433	1
Director Air Force Materiel Laboratory ATTN: AFML-DO-Library Wright-Patterson AFB, Ohio 45433	1
Director, Army Materials and Mechanics Research Center ATTN: DRXMR-PL DRXMR-MT, M. Farrow Watertown, Massachusetts 02172	1 1
Commander White Sands Missile Range ATTN: STEWS-AD-L White Sands Missile Range, New Mexico 88002	1
Deputy Commander US Army Nuclear Agency ATTN: MONA-ZB Fort Bliss, Texas 79916	1
Jet Propulsion Laboratory California Institute of Technology ATTN: Library/Acquisitions 111-113 4800 Oak Grove Drive Pasadena, California 91103	1
Sandia Laboratories ATTN: Library P. O. Box 969 Livermore, California 94550	1
Commander US Army Air Defense School ATTN: ATSA-CD-MM Fort Bliss, Texas 79916	1
Technical Library Naval Ordnance Station Indian Head, Maryland 20640	1
Commander US Army Materiel Development and Readiness Command ATTN: DRCRD DRCDL 5001 Eisenhower Avenue Alexandria, Virginia 22333	1 1
IIT Research Institute ATTN: GAGIAC 10 West 35th Street Chicago, Illinois 60616	1
Commander US Army Materiel Development and Readiness Command ATTN: DRCMT Washington, D. C. 20315	1
Headquarters SAC/NRI (Stinfo Library) Offutt Air Force Base, Nebraska 68113	1
Commander Rock Island Arsenal ATTN: SARRI-RLPL-Technical Library Rock Island, Illinois 61201	1
Commander (Code 233) Naval Weapons Center ATTN: Library Division China Lake, California 93555	1
Department of the Army US Army Research Office ATTN: Information Processing Office P. O. Box 12211 Research Triangle Park, North Carolina 27709	1
ADTC (DLDSL) Eglin Air Force Base, Florida 32542	1
University of California Los Alamos Scientific Laboratory ATTN: Reports Library P. O. Box 1663 Los Alamos, New Mexico 87545	1

DISTRIBUTION (Continued)

	No. of Copies
DRDMI-EA	2
DRDMI-EAA	2
DRDMI-EAS	1
DRDMI-EAM	1
DRDMI-EAP	1
DRDMI-EAB	1
DRDMI-TB	1
DRDMI-ICBB	1
DRDMI-EAT	1
DRDMI-RPR	1

		No. of Copies
DRSMI-LP,	Mr. Voigt	1
DRDMI-X		1
DRDMI-T,	Dr. Kobler	1
DRDMI-TL,	Mr. Lewis	1
DRDMI-TLA,	Mr. Pettey	1
DRDMI-TLA,	Mr. Schaeffel	98
DRDMI-TB		3
DRDMI-TI	(Record Set)	1
DRDMI-TI	(Reference Copy)	1